Novel properties exhibited by films of gold nanoparticle–polythiophene blends

K. Vijaya Sarathy and K. S. Narayan*

Chemistry and Physics of Materials Unit, Jawaharlal Nehru Center for Advanced Scientific Research, Jakkur P.O., Bangalore 560 064, India

Films formed by gold nanoparticle–polyoctylthiophene blends exhibit interesting structure-related properties. Microscopy studies reveal large-scale fluorescent structures spanning 1–2 microns in length, which are modulated by the metal nanoparticle distribution. Fluorescence spectroscopy measurements of the films with different concentrations of the polymer relative to the nanoparticles show interesting changes in the polymer emission bands.

CONJUGATED polymers such as derivatives of poly-paraphenylenevinylene and polylthiophene have appreciable photoluminescence (PL) efficiency and provide a viable option as the active medium in light emitting diodes[1,2]. The formation of optical quality polymer films processed from common solvents on different substrates is a significant advantage for these polymer-based devices. Another class of materials where interesting electronic, optical and structural properties have been recently observed are metal nanoparticles[3]. The nanoparticles can be chemically stabilized by the use of alkanethiols, which render them extremely inert and enable observation of particle size-dependent features. The combination of metal nanoparticles and conducting polymers in the field of molecular electronics has been studied recently, to demonstrate concepts such as molecular bridges between metal clusters[4]. In this paper we report initial studies of complex film patterns obtained from solutions of Au nanoparticles and polyoctylthiophene (P3OT) in solvents where nanoparticle stability and polymer solubility is assured. The possibility of Au nanoparticle interacting with thiophene in the polymer, leading to conformational/structural rearrangement of the polymer chains at the phase boundaries, is probed. The two phases in the films can be easily distinguished using optical microscopy because of the contrasting fluorescent properties, but, the observable length scales are however Rayleigh limited (~ l /2). The structure of the composites and the distribution of the nanoparticles as revealed by transmission electron microscopy (TEM) and scanning electron microscopy (SEM) are also reported.

Blends of the Au–P3OT system were first prepared starting with Au organosol. The organosol containing nanoparticles of Au were synthezised[5] by the initial transfer of 3.0 ml of a 30 mM stock solution of $HAuCl_4$ from aqueous medium to toluene medium using 0.21 g of tetra-*n*-octyl ammonium bromide. This was followed by the reduction of the complexed Au ions in toluene using 2.5 ml of 0.4 M $NaBH_4$ solution, accompanied by vigorous stirring. The resulting dark red organosol was then repeatedly washed with water to remove any traces of the reducing agent (confirmed using X-ray photoelectron spectroscopy

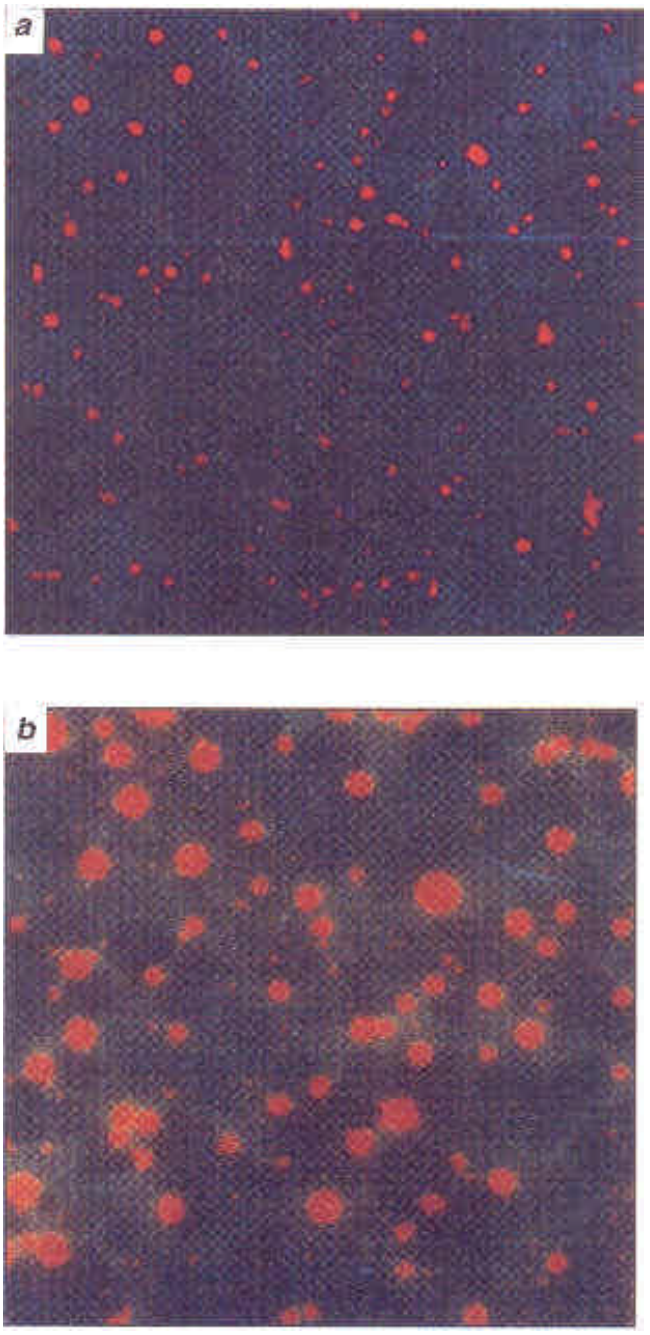

Figure 1 *a*, *b*. Optical microscope images of Au–P3OT films with two different ratios (images viewed under 400 × magnification).

*For correspondence. (e-mail: narayan@jncasr.ac.in)

studies). P3OT was obtained from Aldrich, and was dissolved in *p*-xylene in a weight–volume ratio of 2.0 mg per ml. Blends of Au–P3OT with two different ratios were obtained by the addition of polymer solution to the Au sol (0.8 ml and 1.6 ml of P3OT per ml of Au organosol). The resulting homogenous solution was stable over a period of several days with no phase separation visible due to aggregation/ coagulation of the nanoparticles. In order to prepare Au nanoparticles having a lower size, the reducing agent employed was decreased to one-fifth of its initial amount in the above procedure. Blends were formed similar to the procedure followed for larger Au particles. Thin films on pre-cleaned glass substrates were deposited by spin coating and casting methods.

Optical microscopy was performed using an Olympus B2020 in epi-fluoroscence mode. A Leica S440i instrument was used for SEM studies. The histograms of the features seen in SEM studies were obtained using a Quantimet Image Analyser. TEM images were recorded with a JEOL-3010 microscope operating at 300 keV. For this purpose, the sample was prepared by placing a drop of the blend on a holey carbon grid (3 mm diameter) and subsequently evaporating it before introducing the grid into the microscope.

Large-scale morphological features were observed using optical microscopy. Randomly distributed circular features with sharp intensity contrast were present throughout the film, indicating distinct phases. The fluorescence from the circular regions was observed using different filters and different excitation wavelengths. The emission from these circular regions visually resembled the emission from a pristine polymer film which has an emission maxima centred at 680 nm (ref. 6). The size and the aural density of the circular regions are controlled by the polymer concentration with respect to gold nanoparticle as shown in Figure 1. The diameter of the fluorescing circular spots scales with the amount of the polymer concentration as evidenced by images of films with different polymer concentration in Figure 1 *a* and 1 *b*. Several other films with varying concentrations were also studied to verify this trend of increase in spot size with polymer content. The fluorescence from the spots under prolonged excitation decreases due to a bleaching process.

SEM observations provide further quantitative insight of the phase distribution with a measure of the actual sizes of the circular features. Figure 2 shows the SEM images of Au–P3OT blend where the polymer concentration is high.

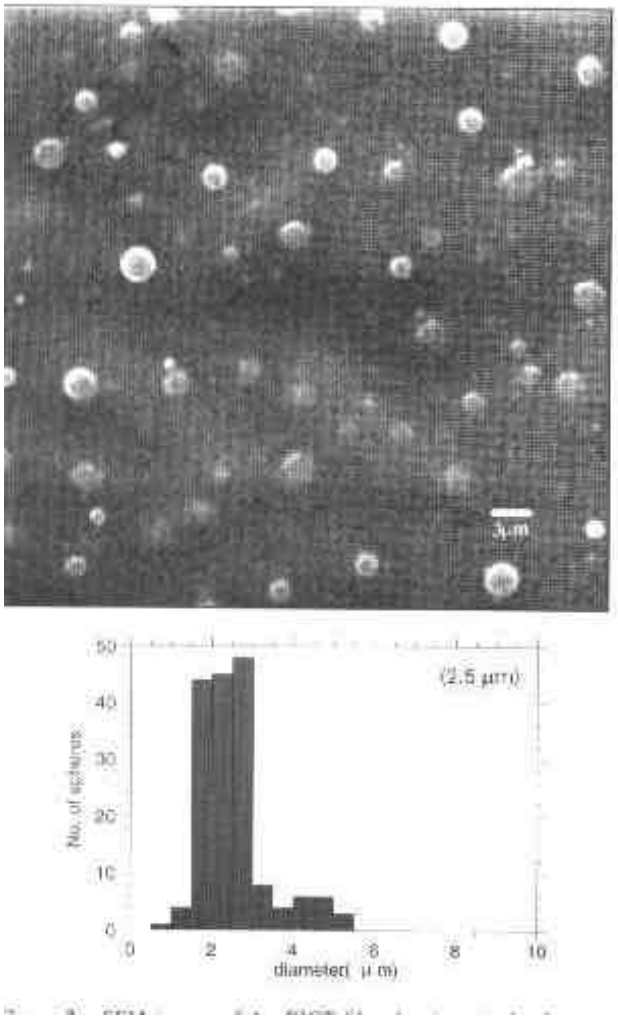

Figure 2. SEM images of Au–P3OT film showing circular features. Variation in the diameters of these features is depicted in the histogram.

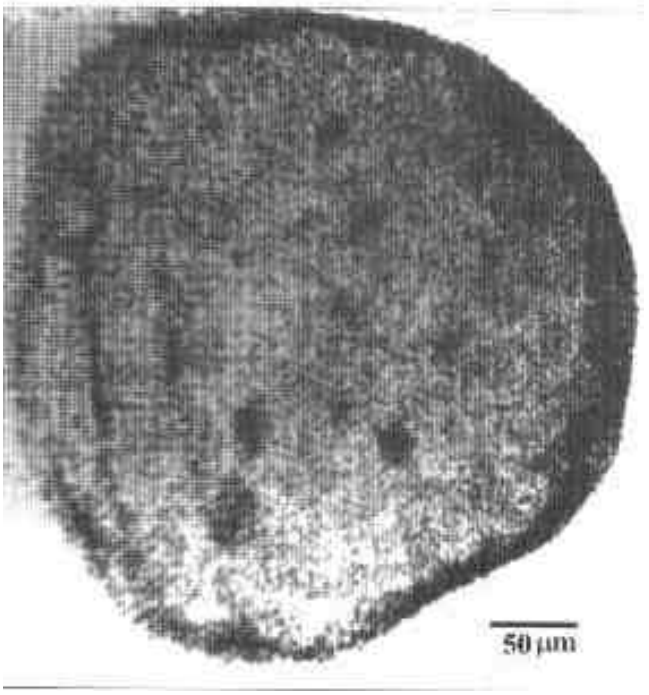

Figure 3. TEM images showing the internal morphology of the circle-like formation wherein the mean diameter of Au nanoparticles seen are ~ 7 nm.

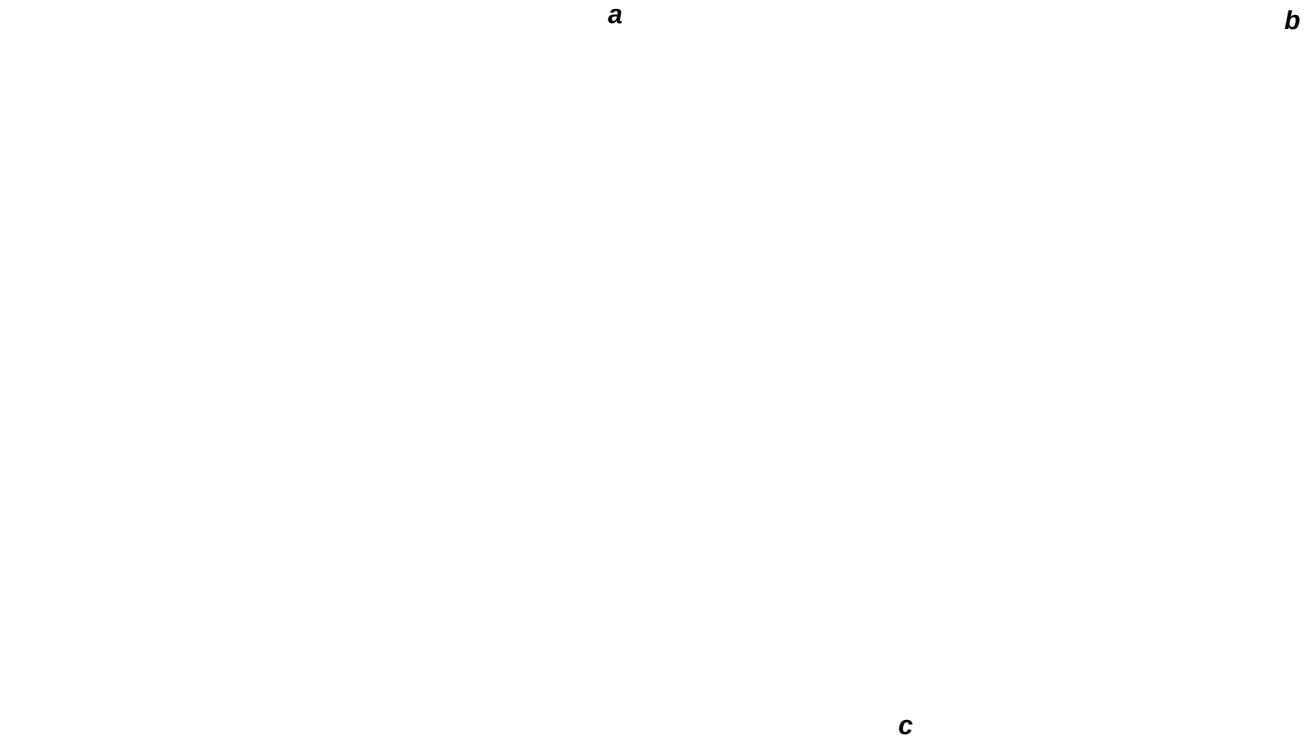

Figure 4. Confocal microscope fluorescence images of the composite films with (***a***) high and (***b***) low concentration of the polymer P3OT; ***c***, typical far field PL spectra of the blends.

The dispersion of the circles could be a signature of the differences in the evaporation/dewetting processes of the two systems during the film formation, resulting in the creation of local domains. The average diameters of the circles are shown in Figure 2, corroborating our observations in the optical studies.

Figure 3 depicts the TEM image of a typical circular region of 0.5 μm diameter in blends with high polymer concentration. A closer observation of the TEM micrograph reveals nanoparticles with an average diameter ~ 7 nm, corresponding to the gold nanoparticle size, clustered in the circular regions. The concentration of the nanoparticles increases radially and is quite dense at the periphery, forming a ring-like structure. Rings with a hole in the centre resembling a doughnut have also been recently observed in other systems[7]. The distribution probably can be explained on the basis of competing processes in the film formation involving solvent evaporation, aggregation of the polymer chains, mobility of the nanoparticles as well as atomic level interactions between the gold and the polymer. Another feature observed in TEM studies, where the thin film of the blend is held in the holey carbon grid, is that the average sizes of the circular regions obtained were less than those observed with optical and SEM images. This feature can have its origin in the formation of films in the absence of solid substrate and which are suspended in the grid with no constraint.

Fluorescent imaging of the film was carried out using a confocal microscope (Biorad Inc.), which has improved lateral and depth resolution compared to non-confocal optical microscopy techniques. The image was recorded for the blend (particles have a mean diameter of ~ 4.0 nm as

obtained from TEM) with a high polymer concentration employing a red and a green band pass filter. The image clearly shows contribution in both the spectral regions. A real colour image constructed from these components is shown in Figure 4 *a*. The general trend is that the circular regions are primarily red with yellow contribution appearing at the periphery and outside the circular region. Another feature observed is the decrease of area with the yellow component in films with lower polymer concentration as shown in Figure 4 *b*. Far field photoluminescence spectral response of these films is consistent with the optical microscope images as shown in Figure 4 *c*. Apart from the normal PL contribution from the polymer with a $\lambda_{max} \sim 680$ nm, a distinct blue-shifted component yielding responses in the region $520 \text{ nm} < \lambda < 600$ nm is present. The 680 nm centred emission is the expected singlet exciton radiative decay of the regio-regular polymer[6]. A blue-shifted emission can arise from subtle changes in the polymer orientation, conformation or packing density due to the presence of the nanoparticles leading to changes in the electronic structure. A more direct change in the electronic density can occur if the interaction between the Au nanoparticles and the polymer interaction is appreciable, leading to charge transfer. Detailed spatially resolved fluorescence measurements are in progress along with high resolution TEM studies to probe the novel properties and unique patterns of the composite films. The fluorescence stability of the polymer in the nanoparticle environment is also being probed along with FTIR studies.

In conclusion, novel morphological and fluorescent features were observed in Au nanoparticle–P3OT composite films. The features varied with the relative concentration of the polymer with respect to the nanoparticle. The difference in the PL spectra of the blend and the pristine polymer is indicative of an interaction between the polymer and the nanoparticles.

1. Burroughs, J. H., Bradley, D. C., Brown, A. R., Marks, R. N., Mackay, K., Friend, R. H., Burn, H. and Holmes, A. B., *Nature*, 1990, **347**, 539.
2. Tessler, N., Harrison, N. T. and Friend, R. H., *Adv. Mater.*, 1998, **10**, 64.
3. Kreibig, U. and Vollmer, M., *Optical Properties of Metal Clusters*, Springer Series in Materials Science-25, 1995.
4. Brousseau III, L. C., Novak, J. P., Marinakos, S. M. and Feldheim, D. P., *Adv. Mater.*, 1999, **11**, 447.
5. Brust, M., Walker, M., Bethel, D., Schiffrin, D. J. and Whyman, R., *J. Chem. Soc., Chem. Commun.*, 1993, 96.
6. Chen, T.–A., Wu, X. and Rieke, R. D., *J. Am. Chem. Soc.*, 1995, **117**, 233.
7. Ohara, P. C., Heath, J. R. and Gelbart, W. M., *Angew. Chem., Int. Ed. Engl.*, 1997, **36**, 1077.

ACKNOWLEDGEMENTS. We acknowledge the valuable guidance of Prof. C. N. R. Rao during the entire project. We also thank Dr S. Meyer and Mr R. Sharma for confocal microscope measurements.

Received 8 July 1999; revised accepted 21 July 1999

Some aspects of presence of lead in the Delhi iron pillar

R. Balasubramaniam

Department of Materials and Metallurgical Engineering, Indian Institute of Technology, Kanpur 208 016, India

Some aspects related to the presence of lead in the Delhi iron pillar are presented in this communication. The presence of a lead solder in the joint between the decorative bell capital and the main body of the Delhi iron pillar has been confirmed by X-ray diffraction analysis of the corrosion product obtained from the joint region. The corrosion products were unambiguously identified as lead carbonate hydroxide hydrate $PbCO_3.Pb(OH)_2.H_2O$ and lead oxide carbonate Pb_2CO_4. The use of lead-based solders in joining the Delhi iron pillar's main body with the decorative bell capital is clearly established. The galvanic corrosion of iron in a lead–iron couple in soil and aqueous (3.5% NaCl solution) environments has also been studied in order to understand the nature of corrosion of the Delhi iron pillar in the buried underground regions. The corrosion of iron in soil was higher than that in the aqueous solution and the iron covered with larger area fraction of lead was corroded to a greater extent in both the environments. Severe localized corrosion of iron was observed at the defects in the lead coating. Based on the simulation experiments, it is concluded that the iron in the buried regions of the pillar is subject to severe localized corrosion due to the presence of lead coating in this region. It is recommended that the lead coating be removed and replaced with a zinc coating for the long-term preservation of the Delhi iron pillar.

THE Delhi iron pillar situated in the *Quwwat-ul-Islam* mosque complex near the Qutub Minar at New Delhi, India is widely popular for its excellent resistance to corrosion. It is a classic product of the forge welding technique used by ancient Indians to manufacture large iron objects. The material of construction of the pillar is almost pure iron with entrapped slag inclusions, which result due to the process of extraction of iron. There are several studies reported in the literature on the corrosion resistance of the pillar[1–3]. The history of the pillar[4,5], its dimensional analysis[4,6], its decorative bell capital[6] and the possible manufacturing technology employed to construct the pillar[7] have been addressed earlier. The presence of lead at several locations on the pillar has been recently addressed in detail[8] wherein visual evidences were presented. The presence of lead sheet at the bottom of the pillar is known from excavation reports[9,10]. The presence of lead appearing as black fillings between some of the iron lumps can be easily noticed on the surface of the pillar. The presence of a lead coating on a part of the surface of the pillar, in the buried underground

e-mail: bala@iitk.ac.in

regions, is noticed by the layer of lead applied on the circumference of the pillar where it intersects the stone platform[8] and also from excavation reports[10]. Conclusive evidence for the presence of lead in the upper regions of the iron pillar, specifically in the joint region between the main body and the decorative bell capital, is presented in this study.

In the buried underground region, the pillar is coated with lead. This lead coating was not provided when the pillar was installed in the *Quwwat-ul-Islam* mosque in the 11th century AD[8]. Rather, it was laid around the pillar's buried underground region when Beglar explored the underground region of the mosque courtyard in the last century[11]. Beglar also constructed the stone platform currently surrounding the base of the pillar in the last century[4]. When the pillar was once again excavated in 1961, during the centenary year of the Archaeological Survey of India, the lead coating previously present on the pillar bottom region was removed. After cleaning the surface of the iron in the buried underground region, a new lead coating was provided to the iron pillar. The lead-coated bottom region of the pillar was again buried in the 1960s[10]. This lead coating was provided much against the wishes of Lal, the Chief Chemist of the ASI[10], as he was aware of the problem of enhanced corrosion of iron in galvanic contact with lead. When two dissimilar metals are in direct contact in a corrosive environment, the active member in the couple corrodes at the expense of the noble member. This form of corrosion is termed galvanic corrosion. As this is a well-known phenomenon in corrosion, it is expected that iron in the buried regions of the pillar must be subjected to enhanced corrosion. The corrosion is insidious in nature, as the nature of corrosion cannot be monitored, because it occurs out-of-sight in the underground region. The secondary aim of the present paper is to also elucidate the deleterious effect of the lead coating in the pillar's buried underground regions. A series of experiments were conducted to simulate galvanic corrosion of iron in contact with lead and the present communication also reports the results of this study.

The decorative bell capital and the main body of the Delhi iron pillar were analysed in detail for surface rusting characteristics[12]. It was noticed that the region at the joint of the decorative bell capital and the main body of the pillar was black in colour, quite different from the colour of magnetite. Moreover, in some locations of the joint, the black filling was covered with a thick corrosion product that was white in colour. Figure 13 in the article by Balasubramaniam[8] shows the joint section in which the presence of the white corrosion product is clearly shown. There was one location where a relatively large lump of the white corrosion product was found and a minute amount of this lump was scraped out of the substrate using a plastic scraper. The corrosion product was ground into a fine powder and used for obtaining X-ray diffraction (XRD) patterns. The diffractograms were obtained in a Rich–Seifert 2000D Diffractometer using CuK_a radiation. Diffratograms were obtained by scanning from 2θ value of 10 to 100 degrees at a speed of 3 deg/min. The diffraction patterns were highly reproducible and they were analysed to obtain information about the nature of the corrosion product.

In order to simulate galvanic corrosion between iron and lead, iron coupons coated with lead were utilized. Coupons (2 cm × 1 cm × 0.4 cm) of mild steel were prepared and the surfaces of the coupons were thoroughly cleaned to remove scales and greasy matter. Fine emery papers were not used and the final surface finishing was stopped at 1/0 emery paper. Lead was melted in a crucible in a furnace kept at 450°C. Zinc chloride and ammonium chloride, which act as flux, were added to the crucible so that molten lead may adhere to the surface of the mild steel. The iron coupons were dipped in the molten crucible bath for obtaining the lead coating. In order to study the area effect in galvanic corrosion between iron and lead, the mild steel coupons were coated such that specimens having relative area of iron and lead in the ratios of 3 : 1 and 1 : 1 were obtained. One set of the samples (i.e. iron : lead specimens of 3 : 1 and 1 : 1 area ratio) was completely immersed in a 3.5 wt% NaCl solution and another set was buried in loamy soil which was drenched every 24 h with half a litre of the same solution. The solution used in the study was 3.5% NaCl because it is reported that the soil in the vicinity of the buried underground regions of the Delhi iron pillar is loaded with soluble sulphates and chlorides[10]. As sulphates are beneficial to the corrosion of lead[13], sodium chloride solution was chosen for the study. The soil, in which the lead-coated steel coupons were buried, was drenched with half a litre of 3.5% NaCl solution once every day. After every 24 h, the samples were taken out from the soil and from the constant immersion condition, thoroughly cleaned in running water with the help of a brush and the weight loss was noted. The corrosion rate (in mpy = mils per year) was estimated by assuming that only the iron member in the galvanic couple corroded and by utilizing the following equation:

$$\text{Corrosion rate (mpy)} = (534W)/(ADT),$$

where W is the weight loss in mg, A is the area in square inches, D is the density in gm/cc and T is the exposure time in hours. The samples were also periodically observed in a scanning electron microscope (JEOL JSM840A) in order to understand the nature of galvanic corrosion of iron. The observations were conducted in the lead-coated regions, at the interface between the lead coating and iron, and in the uncoated iron regions.

The diffraction pattern obtained from the white corrosion product is provided in Figure 1. The maximum peak occurred around $2\theta = 26.9°$. The background radiation was subtracted and the relative intensities of the peaks were

obtained. The XRD data were analysed with the atmospheric corrosion products of iron, lead, copper and tin using JCPDS diffraction files[14]. Moreover, all the corrosion products consisting of Fe, Pb, Cu, Sn, O, C, S and H were investigated. The JCPDS data of oxides and oxyhydroxides of iron were especially carefully compared. The maximum intensity peaks in the case of iron oxyhydroxides/oxides are concentrated in the 2θ range between 30° and 35°. The maximum intensity peak in the experimental pattern did not contain such peaks. The additional fact that the corrosion product was white in colour also diminished the possibility that it could be an oxyhydroxide/oxide of iron.

All the diffraction peaks of the experimental pattern matched with those of the compounds lead carbonate hydroxide hydrate $PbCO_3.Pb(OH)_2H_2O$ (JCPDS file number 09–0356) and lead oxide carbonate Pb_2CO_4 (JCPDS file number 17–0729). It is interesting to note that the theoretical relative intensities also matched with the experimental intensities (Table 1). It is not surprising that lead carbonate hydroxide hydrate was identified as it is the most common atmospheric corrosion product of lead[15]. The peaks that were identified with these two compounds have been marked in Figure 1.

Table 1 gives the thermodynamic free energy values for some of the common atmospheric corrosion products of lead[16]. In the absence of sulphur in the atmosphere, one of the most stable corrosion products of lead at room temperature is lead oxide carbonate. Therefore, the presence of a major portion of this phase in the corrosion product is not surprising. It must be noted that the compounds identified (namely lead carbonate hydroxide hydrate and lead oxide carbonate) are compositionally identical except for the state of hydration. For example, the chemical formula of lead carbonate hydroxide hydrate can be rewritten as $PbCO_3.PbO.2H_2O$, which is similar to $Pb_2CO_4.2H_2O$. Therefore, lead carbonate hydroxide hydrate can be viewed as lead oxide carbonate with a higher degree of hydration.

Incidentally, the other locations where lead-based solders have been used have also been outlined earlier[8]. These locations are generally in the decorative bell capital of the pillar[6]. Several joints between the individual decorative bell capital components contain evidence for the use of lead-based solders.

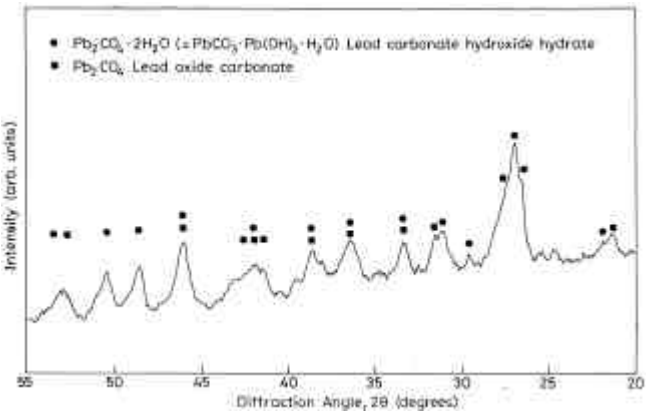

Figure 1. X-ray diffraction pattern of the corrosion product obtained using CuK_a radiation.

Figure 2 provides the corrosion rates as a function of time for the steel coupons with 25% and 50% of surface area coated with lead, in both the aqueous solution and soil conditions. The corrosion rate of iron in the buried soil conditions is higher than that for complete immersion in the aqueous solution, for both specimens. Moreover, corrosion rate for the steel coupon with 50% surface area coated with lead is higher than that for the coupon with 25% surface area coated with lead, in both the environments. It is also noted that the corrosion rate is relatively higher in the initial stages and later decreases with time in all the cases.

It is known that when two metals are coupled together and exposed to a corrosive environment, the active metal in the couple corrodes at the expense of the other, thereby sacrificially protecting the nobler metal. The indication of an active metal and a noble metal can be obtained from the electromotive force (EMF) series, where pure metals are classified and arranged according to their electrode potentials in certain defined conditions. Under ideal conditions, these reduction potentials provide an indication of the relative ease with which a metal would corrode. The element with a more negative reduction potential is more prone to corrosion compared to an element with a less

Table 1. Analysis of experimental XRD pattern

2θ (exptl)	I/I_0 (exptl)	Phase	hkl	2θ (theoret.)	I/I_0 (theoret.)
21.5	28	LCHH	112	20.8	90
21.9	22	LCHH	113	22.4	80
26.6	72	LCHH	204	26.7	100
27.2	100	LOC	–	27.7	100
28.0	42	LOC	–	28.0	95
29.5	20	LCHH	116	29.3	80
30.8	23	LCHH	108	30.9	70
31.2	39	LOC	–	31.3	60
33.4	33	LCHH	214	33.5	10
		LOC	–	33.8	20
36.4	40	LCHH	00 10	36.2	90
38.7	36	LCHH	119	38.1	10
		LOC	–	38.6	20
39.7	20	LCHH	221	39.7	70
		LOC	–	39.4	30
		LOC	–	40.0	35
41.5	27	LOC	–	41.3	35
41.8	33	LCHH	311	41.5	70
		LOC	–	41.8	16
42.3	30	LCHH	224	42.4	20
46.3	55	LCHH	316	46.9	50
		LOC	–	47.0	16
48.6	40	LCHH	317	48.7	50
50.5	38	LCHH	21 11	50.6	90
52.9	26	–	–	–	–
52.9	26	LOC	–	52.9	25
53.8	12	LCHH	21 12	53.9	20

LCCH = lead carbonate hydroxide hydrate, $PbCO_3.Pb(OH)_2.H_2O$.
LOC = lead oxide carbonate, Pb_2CO_4.

negative potential. This is also understandable from the idea that when a metal is prone to corrosion, it would dissolve as ions, in the process leaving behind an excess of charge in the metal. Therefore, the metal that is more prone to corrosion would leave behind more electrons and thereby this metal would possess a lower electrode potential, analogous to the concept of potential in electricity. The EMF series is not as practical as the galvanic series, which provides the actual arrangement of the metal and alloys, which will corrode in a certain environment. The galvanic series is more practical as alloys in different environments can also be compared. The galvanic series is usually obtained for sea water or simulated sea water (3.5 wt% NaCl solution). The position of lead with respect to iron in the galvanic and EMF series should be noted in order to understand the galvanic effect of coupling lead to iron in affecting the corrosion behaviour of iron.

In the EMF series, the reduction potential for lead is higher (– 0.126 V versus standard hydrogen electrode, SHE) than that for iron (– 0.440 V versus SHE) thereby implying that when pure iron and lead are in contact, under ideal conditions, iron should corrode at the expense of lead[13]. This assumes that the area of exposure of iron and lead is the same and that they are exposed under ideal conditions, for which the EMF series is defined. In the galvanic series, it is also seen that lead is noble compared to iron (and steel) and this implies that iron should corrode in a couple made of iron and lead when exposed to sea water (the usual environmental condition for which the galvanic series is reported).

Lead could affect galvanic corrosion of the pillar's iron in the following ways:

(i) Affecting the exchange current density of reduction processes – The likely reduction reactions that can take place on the surface are either the reduction of hydrogen or that of oxygen. The exchange current density for these reduction reactions could be modified in the presence of lead. It is noticed that the exchange current density for the above reactions are much more lower on lead compared to iron[13] and therefore, the effect of lead in modifying the exchange current density, and subsequently affecting galvanic corrosion, would not be significant.

(ii) Affecting the anode–cathode area ratio – The area effect is very important while discussing galvanic corrosion. In case the anode area is much smaller than the cathode area, corrosion of the anode will be severe, as a large cathodic area demands a large anodic current, which must necessarily come from a small anode area. However, if the anode area is much larger than the cathode area, the intensity of corrosion is spread over the larger surface area of the anode and therefore, corrosion is not severe or damaging. The experimental corrosion rates (Figure 2) clearly indicate the area effect as the iron coupons with larger surface area of lead coverage are corroded more. Microstructural observation of the surface of the corroded specimen clearly showed that severe localized corrosion of iron was observed in the specimens exposed in the soil environment. Moreover, localized corrosion was observed particularly in areas where there were defects in the lead coating (Figure 3). On the other hand, corrosion of iron in the uncoated areas was relatively uniform. The severe localized corrosion of iron at the lead coating defects is clearly indicative of the area effect in galvanic corrosion. Therefore, the lead coating on the iron pillar in the buried underground region is deleterious. This is also corroborated by the observations of Ghosh[9] and Lal[10] that the iron in the buried underground region was corroded much more severely compared to iron in the exposed surface. Lal also noted that the coating of lead in the buried underground regions was uneven (with a mean thickness of 3 mm). The

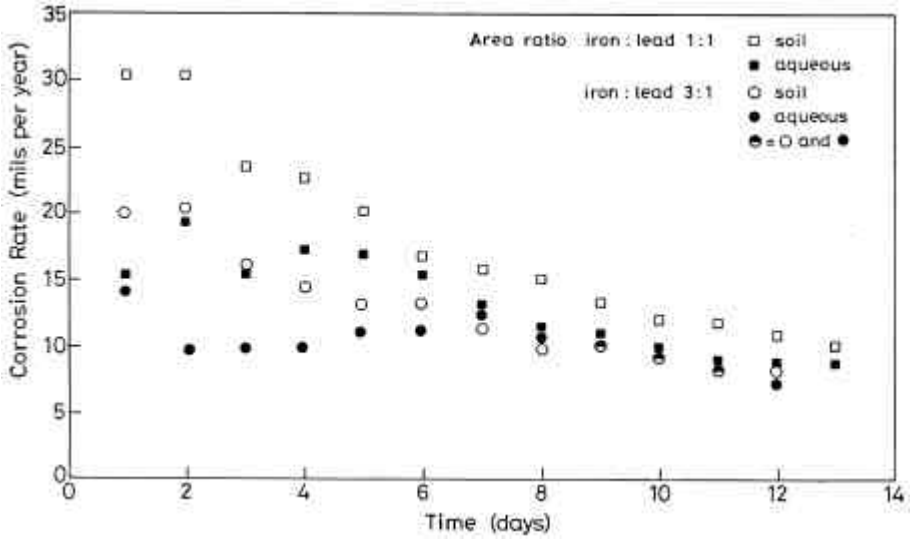

Figure 2. Corrosion rate as a function of time for steel sample with 25% and 50% of area coated with lead for complete immersion in 3.5% NaCl solution and soil corrosion conditions. The soil was drenched every 24 h with half a litre of 3.5% NaCl solution.

lead coating was found to be in an excellent state of preservation[10]. However, the buried portion was found covered with rust layers ranging from a few mm to 15 mm[9,10]. Interestingly, numerous cavities and corrosion pits were also observed in the buried region and this must have resulted due to the localized corrosion taking place at the coating defects in the lead coating. It is also interesting at this junction to note that lead also appears in the Delhi iron pillar's exposed surface in the form of fillings between some iron lumps[8]. As the area of exposed surface of the Delhi pillar iron is much more than that of lead filling observed at different locations in the pillar, the anode area is much larger than the cathode area. This will not result in destructive galvanic corrosion of iron in the exposed surface of the pillar, as has been the case. Apart from the area effect in galvanic corrosion, another important effect is the distance effect. The galvanic corrosion of the active member in the galvanic couple would be maximum at the interface between the members of the couple as this is the location where solution/soil resistance would be minimum. As per expectations, severe localized corrosion was also observed at the interface between the lead coated and uncoated surface (Figure 4) in all the coupons. The corrosion at the interface was much more severe in the case of soil burial conditions than in aqueous immersion conditions.

(iii) Adding an extra input to the cathodic reduction reaction – On a microscopic scale, lead could positively influence corrosion of the Delhi iron pillar in the atmosphere-exposed regions in the following way and, in fact, be beneficial to the pillar's corrosion resistance. Normally, the cathodic reaction occurring on the surface of lead is either hydrogen or oxygen reduction. An additional reaction that could occur (although very unlikely) on the surface is the reduction of lead ions. All these reactions would add an extra input in the form of an additional cathodic current to the cathodic current already flowing in the circuit. In such a case, this effect is similar to the effect of adding a cathode to an active–passive anode on the corrosion behaviour[17]. By the addition of an extra input into the cathodic reaction, the induction of passivity may be accelerated as it was shown in the case of slag particles present in the pillar's iron[2,3]. Therefore, coupling of lead could aid the induction of passivity, in the case of an active–passive metal in contrast to its effect on an active metal, where it would accelerate the corrosion rate.

In view of the deleterious nature of the lead coating in the buried underground region, it is highly recommended that the lead coating be removed and replaced with a zinc coating which can also sacrificially protect the iron in the buried underground regions. Iron in the buried underground region is currently subjected to intense galvanic corrosion. It is important to replace this lead coating with a zinc coating for proper preservation of this important cultural and scientific monument. A proposal to replace the lead coating with a zinc coating has also been previously placed by Lal[10] and Anantharaman[18].

The presence of a lead solder in the joint between the decorative bell capital and the main body of the Delhi iron pillar has been confirmed by analysis of the corrosion product obtained from the joint region. It has been shown by XRD that the corrosion products were lead carbonate hydroxide hydrate and lead oxide carbonate. The results of the study clearly establish the use of lead-based solders in the joining operations of the Delhi iron pillar's main body with the decorative bell capital. The galvanic corrosion of iron in iron–lead couples under soil and complete immersion conditions has also been studied. It was observed that the corrosion of iron was higher in soil than that in the aqueous 3.5% NaCl solution and that the iron covered with larger area fraction of lead was corroded to a greater extent in both the environments. Severe localized corrosion of iron was observed at the coating defects in the lead coating,

Figure 3. Localized corrosion of iron at the defects in lead coating for steel sample with 25% of area coated with lead in soil corrosion conditions.

Figure 4. Severe localized corrosion of iron at the interface between lead-coated and uncoated regions for the steel sample with 25% of area coated with lead in soil corrosion conditions.

Table 2. Enthalpies, entropies and free energies of formation of several lead compounds at 298 K (ref. 16)

Compound	ΔH (kJ/mol)	ΔS (J/deg/mol)	ΔG (kJ/mol)
PbO	– 219.2	66.3	– 238.9
Pb_3O_4	– 718.0	211.8	– 781.1
PbO_2	– 274.2	71.7	– 295.6
PbS	– 98.2	91.3	– 125.4
$PbSO_4$	– 919.2	148.4	– 963.4
$PbCO_3$	– 698.9	130.8	– 737.9
Pb_2CO_4	– 816.0	204.0	– 876.7

especially in the soil environment. Based on these simulation experiments, it is concluded that the iron in the buried regions of the Delhi iron pillar is subject to severe localized corrosion due to the presence of the lead coating in this region. It is highly recommended that the lead coating be removed and replaced with a zinc coating for the long-term preservation of the pillar.

1. Wranglen, G., *Corros. Sci.*, 1970, **10**, 761–770.
2. Balasubramaniam, R., *NML Techn. J.*, 1995, **37**, 123–145.
3. Balasubramaniam, R., *Trans. Indian Inst. Met.*, 1997, **50**, 23–35.
4. Balasubramaniam, R., *Curr. Sci.*, 1997, **73**, ,1057–1067.
5. Balasubramaniam, R., *Bull. Met. Mus.*, 1999, accepted.
6. Balasubramaniam, R., *JOM.*, 1998, **50**, 40–47.
7. Balasubramaniam, R., *Bull. Met. Mus.*, 1999, **31**, 40–63.
8. Balasubramaniam, R., *Bull. Met. Mus.*, 1998, **29**, 20–40.
9. Ghosh, M. K., *NML Tech. J.*, 1963, **5**, 31–45.
10. Lal, B. B., in *The Delhi Iron Pillar: Its Art, Metallurgy and Inscriptions* (eds Joshi, M. C., Gupta, S. K. and Goyal, S.), Kusumanjali Publication, Meerut, 1996, pp. 22–58.
11. Beglar, Y. D., *Archaeol. Surv. India Annu. Rep.* 1871/72, **IV**, 28–30.
12. Balasubramaniam, R., *Bull. Met. Mus.*, 1999, accepted.
13. Uhlig, H. H., *Corrosion and Corrosion Control*, John Wiley, New York, 1963, pp. 310–311.
14. JCPDS Powder Diffraction Files, PCPDFWIN Software, Joint Committee on Powder Diffraction Standards – International Centre for Diffraction Data, Swarthmore, USA, 1996.
15. Jeyraj, V., in *History of Science and Technology in India: Coins and Metallurgy* (eds Kuppuram, G. and Kumudamani, K.), Sundeep Prakashan, New Delhi, 1989, vol. III, pp. 99–103.
16. Kubaschewski, O., Evans, E. L. and Alcock, C. B., *Metallurgical Thermochemistry*, Pergamon Press, New York, 4th edn, 1985.
17. Tomoshov, N. D. and Chernova, G. P., *Passivity and Protection of Metals Against Corrosion*, Plenum Press, New York, 1967, pp. 151–180.
18. Anantharaman, T. R., *The Rustless Wonder – A Study of the Delhi Iron Pillar*, Vigyan Prasar, New Delhi, 1996.

ACKNOWLEDGEMENTS. I thank the Archeological Survey of India for permission to study the Delhi iron pillar. I also thank Mr N. Lakshminarayana for obtaining the XRD diffraction patterns and
Mr A. Singhal and Mr A. P. Singh for conducting weight loss measurements in the aqueous and soil environments, respectively.

Received 19 May 1999; accepted 21 June 1999

Arsenicosis and deteriorating groundwater quality: Unfolding crisis in central-east Indian region

Piyush Kant Pandey*†, Ram Narayan Khare*, Ramesh Sharma*, Santosh Kumar Sar*, Madhurima Pandey* and Pramod Binayake**

*Bhilai Institute of Technology, Durg 491 002, India
**J. L. N. Hospital and Research Centre, Bhilai Steel Plant, Bhilai 490 006, India

We report here the appearance of arsenic and chemical extent of the deterioration in groundwater quality of the Rajnandgaon district of MP. Out of the 390 samples we analysed, 26 sites were found to be contaminated with arsenic. Total arsenic concentration obtained in the analyses ranged between 0.01 and 1.01 mg/l. Statistical analysis shows that the mean concentration of arsenic is about 0.35 mg/l in the village Koudikasa. Our survey shows that about 400 people (30% of the population) are affected and about 130 people are critically affected by arsenic poisoning in a single village. The number of people at risk is about 10,000. The symptoms observed and the age distribution of patients are also presented. Studies on arsenic have shown neither a strong positive correlation with iron concentration nor a strong negative correlation with pH. These results testify the urgent need to study the source profile and the geochemical reactions responsible for the occurrence of arsenic.

ARSENIC is widely present beneath the earth. Arsenic that comes to the surface due to agricultural irrigation and withdrawing underground water, geothermal power plants or mining, has seriously contaminated the environment, particularly in Asia. Groundwater is the main source of drinking water in India and Bangladesh. In the early eighties, arsenic contamination of groundwater was detected in six eastern districts of West Bengal, India. This concentration ranged from 0.06 mg/l to 1.86 mg/l, far in excess of WHO's drinking water provisional guideline value of 0.01 mg/l. It is estimated that over 150,000 people are affected by arsenic and are suffering from 'arsenical dermatosis' (black spots, eruptions and even cracking of skin). Similar problems have also become apparent in Bangladesh in areas bordering India, but their geographical extent is yet to be defined[1].

High concentration of arsenic in groundwater has been reported from the Bengal Delta Plains in West Bengal and Bangladesh[2–8]. Symptoms of arsenicosis are primarily manifested in the forms of different types of skin diseases like skin lesions, hyperkeratosis, melanosis, etc.[9] Arsenic is also the cause of various carcinogenic manifestations. Arsenic contamination and the consequent skin cancer have been reported way back in 1968 (ref. 10). A study on the effect and dose–response relationship of skin cancer and Blackfoot disease with arsenic was then made in Taiwan[11]. Cases of chronic arsenic poisoning were reported from Mexico[12]. Sporadic cases of groundwater

†For correspondence. (e-mail: bitlib@bom6.vsnl.net.in)

contamination have been reported from various parts of the United States[13,14].

In this article, we report the arsenic levels and the clinical manifestations observed in the village Koudikasa of Rajnandgaon district of Madhya Pradesh. Rajnandgaon district is situated in the south-eastern part of MP. The district lies between 20°70' and 22°29'N latitudes and 81°29' and 88°29'E longitudes (Figure 1). Rajnandgaon district is predominantly agrarian having some dense forests. Out of the total geographical area of 1,109,700 ha, the total area of forests in the district is 389,260 ha (35%) and the net sown area is 496,275 ha (44.7%). The state average for forest and arable land is 32% and 42.7% respectively. The site studied is about 8 km from the Chowki town and has an undulating hilly topography. Sheonath, the principal river of the district, originates near Chowki block and is a major tributary of Mahanadi, the biggest river of the central-east India. Demographically, the total population of the district is 1,439,951 (1991 census).

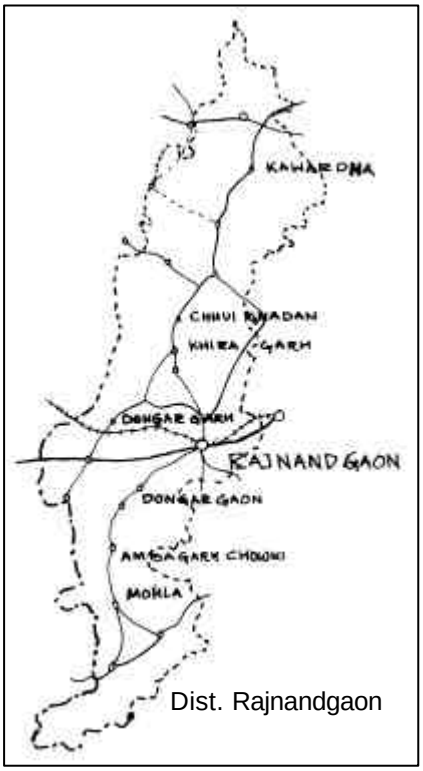

Figure 1. Location map of the Rajnandgaon district.

Except two cities of Rajnandgaon and Khairagarh, the entire district depends on tubewells and dug-wells. Tubewells are fitted either with hand pumps or power pumps. In Ambagarh–Chowki block with about 160 inhabited villages, there are about 500 hand pumps and about 10,000 hand pumps/tubewells in the entire district. This heavy dependence on the groundwater has resulted in over-exploitation and severe deterioration in the water quality. In this study, we have identified one of the major cases of arsenic poisoning in India.

Over-exploitation has resulted in an increase in the depth of the bore from an average 45–50 m to 70–80 m. Even at this depth many bores go dry in the summer and there is deterioration in the water quality. We have carried out analyses on the quality of water supplied mainly by the Public Health Engineering Department (PHED) of MP and private citizens. We report here the chemical extent of the deterioration in water quality.

The conventional analytical methods which have employed include measurements of pH by single electrode pH meter, conductivity and total dissolved solids by conductivity meter, hardness by EDTA titration, chloride by silver nitrate titration, sulphate by turbidity meter, nitrate by brucine method, iron by 1,10-phenanthroline and thiocyanate-surfactant method and manganese by persulphate method, spectrophotometrically and fluoride by SPANDS method. Results are presented in Table 1.

We did not carry out studies on arsenic earlier because there had never been any report of arsenic contamination. Now we have analysed samples for arsenic as its presence was suspected in village Koudikasa based on certain skin pigmentation defects, which were noted during one of our visits for sample collection.

Table 1. Groundwater quality observed in some villages of the Rajnandgaon district

Property	Prescribed standards (all values in mg/l unless indicated otherwise)		Number of samples analysed	Number of samples exceeding permissible limits	Number of samples exceeding excessive limits
	Permissible	Excessive			
Taste/odour	Un-objectionable	Un-objectionable	400	37	250
pH (units)	7.1–8.5	6.5–9.2	250	190	12
Total dissolved solids	500	1500	400	125	39
Total hardness	200	600	250	90	30
Chlorides	200	400	245	131	18
Sulphates	200	400	210	75	19
Fluorides	1.0	1.5	175	25	5
Nitrates	45	45	58	3	1
Iron	0.1	1.0	350	150	70
Manganese	0.05	0.5	50	17	2

Water for the analysis was obtained from the hand pump or the power pump (if it was fitted on the source). The pH, conductivity and total dissolved solids were determined on the site itself. The groundwater was analysed using spectrophotometer (Digispec 110-D) by the silver diethyl dithio carbamate (SDDC) method[15]. Modified Gutzeit apparatus[16] was used for arsine generation. All chemicals used were AR grade (Merck, Germany). The SDDC method is quite sensitive and most of the samples did not require any pre-concentration because of the high concentration of arsenic. Minimum detectable quantity of the SDDC method is 1 μg of arsenic[17]. Some of the samples analysed contained arsenic beyond the range of the method (20 μg max.) and required suitable dilution with double distilled water. Only a

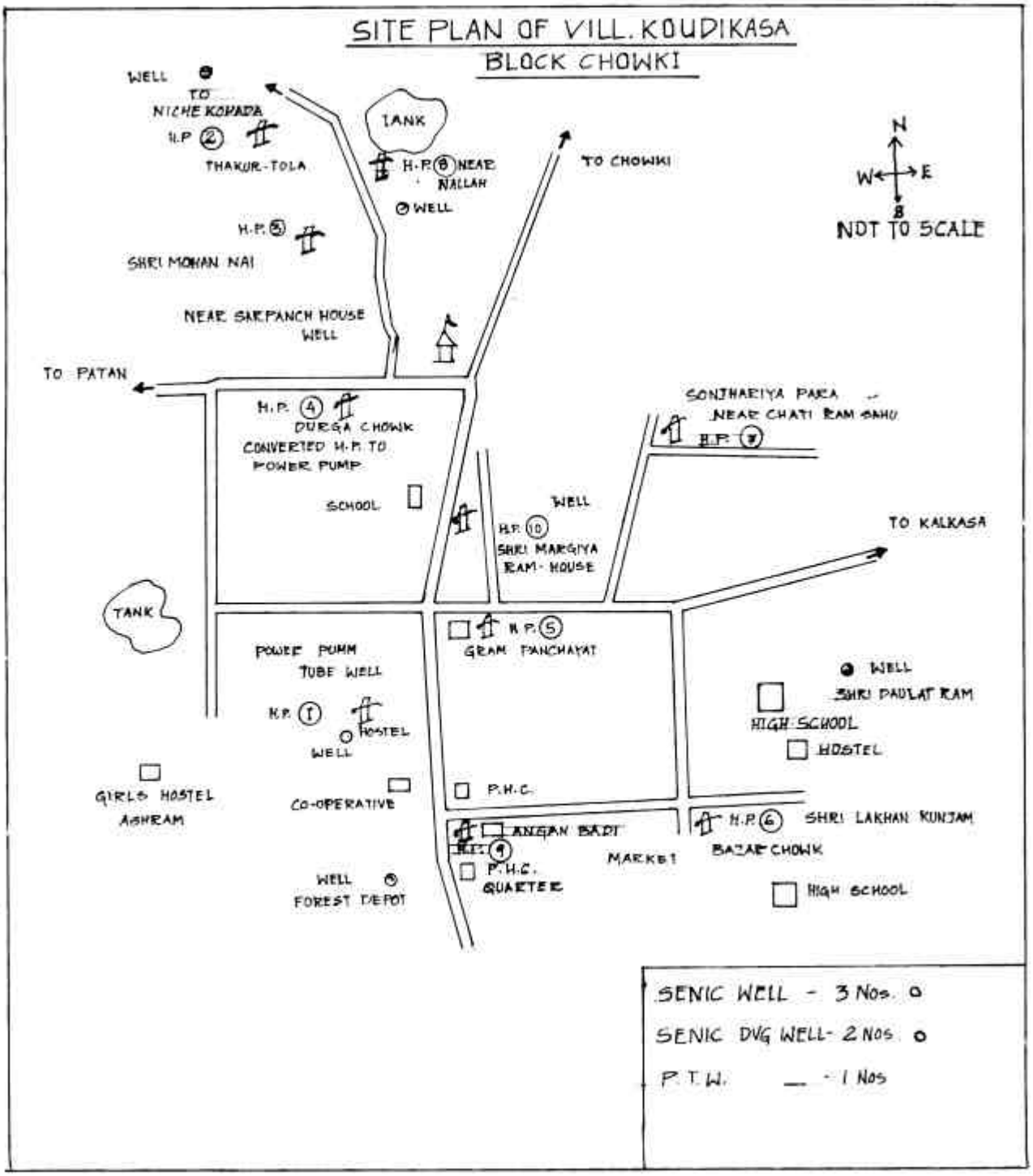

Figure 2. Site map of Koudikasa village depicting the location of water sources.

Table 2. Arsenic in groundwater at village Koudikasa, Dist. Rajnandgaon, MP

Place	Location	Identification no.	Arsenic (mg/l) in January 1999	October 1998	January 1998
Koudikasa village	Bazaar Chowk HP	HP 6	0.89	0.9	1.01
	Forest well	FW	0.53	0.53	0.6
	Grampanchayat HP	HP 5	0.33	0.35	0.36
	Doulat Ram's well	DW	0.15	0.14	0.18
	Power pump	HP 1	0.02	0.02	0.01
	Angan Badi HP	HP 2	0.21	0.22	0.28
	Girls Primary School	HP 10	0.25	0.2	0.19
Dewarsur village	Roadside HP, Dewarsur		0.04	0.03	NA
Mavritola village	Bus stand		0.04	0.04	0.03
Mulethitola village	Gram panchayat		0.05	0.04	0.03
Kunderatola village	New pump		0.02	Not dug	Not dug
Bodal village	Temple HP		0.03	0.03	0.03
	Village HP		0.02	0.03	0.03
Chowki town	Public distribution tubewell		0.02	0.02	
	Town HP		0.02	0.01	NA

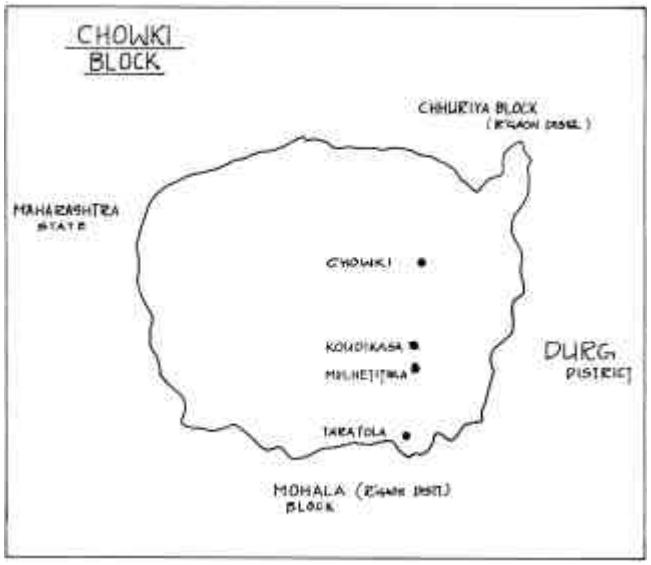

Figure 3. Location map of the Ambagarh–Chowki block and Koudikasa village.

few samples were concentrated by adding acid (0.5 ml conc. HCl)[15] and then boiling to reduce the volume. The results obtained after such a preconcentration are included here only after calculating the percentage recovery in them, as there could be loss of arsenic in the process. Out of 250 samples analysed, 26 sites were found to be contaminated with arsenic. We have restricted ourselves to the study of only a few villages. Total arsenic concentration obtained in the analyses ranges between 0.01 and 1.01 mg/l. Results of analysis of the contaminated sites (Figure 2) are presented in Table 2. Most of the hand pumps in Koudikasa village are contaminated with arsenic. The extent of contamination and its effect on the health of the people there can be estimated from the arsenic concentration in the water supplied through the public distribution system at Ambagarh–Chowki town (about 8 km from Koudikasa, Figure 3) is 0.02 mg/l. The arsenic concentration in this town, though now within the prescribed WHO limit, could further increase because of further contamination of the groundwater. We estimate that about 10,000 people of this region are at risk of being affected by arsenic poisoning. Further, a large adjoining part of central India may also be considered at risk.

Table 3. Statistical analysis of arsenic in groundwater at Koudikasa

	Arsenic (mg/l) in January 1999	October 1998	January 1998
Mean	0.34	0.34	0.38
Standard error	0.11	0.11	0.13
Median	0.25	0.22	0.28
Mode	#N/A	#N/A	#N/A
Standard deviation	0.29	0.30	0.33
Sample variance	0.08	0.09	0.11
Kurtosis	1.59	1.51	1.55
Skewness	1.26	1.27	1.27
Range	0.87	0.88	1.00
Minimum	0.02	0.02	0.01
Maximum	0.89	0.90	1.01
Sum	2.38	2.36	2.63
Count	7.00	7.00	7.00

Variations in the arsenic levels have been noted in January 1998, October 1998 and January 1999. These variations reflect the probable effect of the geo-chemical parameters, sampling biases, etc. Longer seasonal study on the variation in arsenic levels is indicated by these results. The statistical analysis shows that the mean concentration of arsenic is about 0.35 mg/l with a standard deviation of 0.31 (Table 3).

Table 4. Water quality parameters in the village Koudikasa (all values in mg/l unless indicated otherwise)

Parameters	Anganbadi HP 2	Girls Primary School HP 10	Gram-Panchayat HP 5	Bazaar Chowk HP 6	Power Pump HP 1	Doulat Ram well DW	Forest well FW	ICMR recommended maximum concentration
Turbidity, NTU	4	3	2	3	1	4	3	5
Colour (units)	–	–	–	–	–	–	–	5
pH	7.43	7.52	7.54	7.21	6.68	7.43	7.59	7–8.5
Total dissolved solids	174	262	274	213	110	319	205	500 (WHO)
Conductivity, m mhos	0.275	0.396	0.432	0.338	0.175	0.502	0.323	–
ATC, m mhos	0.271	0.391	0.43	0.335	0.171	0.498	0.321	–
Hardness as $CaCO_3$	117.5	205.0	205.0	154.0	70.0	130.0	158.0	300
Calcium as Ca	25.20	39.00	47.00	26.00	9.00	37.00	29.00	75
Magnesium as Mg	13.20	26.00	21.00	21.50	11.50	15.50	21.00	30
Sodium	32	35	41	43	37	87	47	–
Potassium	3	5	4	11	1	11	2	–
Alkalinity	140	190	150	190	90	190	200	–
Chlorides	35	53.0	64.0	35.0	25.0	71.0	32.0	200
Sulphates	236	264	288	256	264	268	252	200
Fluorides	BDL	BDL	BDL	BDL	BDL	BDL	BDL	1
Iron	0.25	0.01	0.01	0.01	0.01	0.01	0.01	0.1

BDL = Below detection limit.

Table 5. Clinical manifestations of arsenicosis observed in the population of Koudikasa

Manifestation	Prevalence (%)	
	Study group (n = 500) %	Control group (n = 500) %
Palmoplanter keratosis	22.50	Nil
Spotted melanosis (Raindrop pigmentation)	18.50	Nil
Diffuse melanosis	16.25	Nil
Dorsal keratosis	15.50	Nil
Leucomelanosis	13.5	Nil
Dry hair and alopecia	10.50*	4.25
Brittle nails	11.25**	3.50
Congestion of nasal mucosa	8.0	2.25
Skin and other malignamy	Nil	Nil

*Other causes of dry hair and alopecia like seborrhoea capititis or iron deficiency were ruled out.
**Other causes of brittle nails like fungal infection were ruled out.

Seven sites from the Koudikasa village were analysed to ascertain the water quality. The results, presented in Table 4, show that hardness of the samples and the presence of calcium, magnesium and sulphates in high concentrations. The results obtained at the various sites in village Koudikasa show a very close correlation with each other. This close correlation can be expected to extrapolate other groundwater sources of the adjoining area and hence should be a cause of concern.

On the basis of these results, we carried out a survey of the village which showed that about 400 people are clinically manifesting signs of arsenicosis (Table 5) and 130 people are critically affected (second to third stage of arsenicosis).

The extent of arsenic poisoning in the area is expected to be quite large. We are now working on the actual estimation of the geographical extent and the population affected.

Clinical symptoms show that a large number of people have developed diffuse palmoplanter keratosis which is a sign of moderately severe toxicity[18]. We have also tested the presence of arsenic in urine samples (results not reported here). The lowest concentration of arsenic in groundwater causing dermatosis and skin lesions is reported to be 0.2 mg/l by Chakraborti *et al.*[9] and Mandal *et al.*[18] corresponding to a daily intake of about 1 mg arsenic. Therefore, even in the absence of the hair and nail analyses the clinical manifestations are certainly a result of the groundwater contamination. Figures 4 and 5 show patients with palmer keratosis (Figure 4) and planter keratosis (Figure 5).

Figure 4. Palmer keratosis (village Koudikasa).

Figure 6 shows that most of very critically affected people are in their early adulthood or middle age, and sex of the patients does not seem to affect the progression of arsenicosis. Most of these people have been residing in the village since birth. A few of the female patients who came to Koudikasa village after marriage have developed symptoms of arsenicosis. However, this does not mean that the children are less affected by arsenic. It only means that the symptoms have not yet manifested to allow identification and the effects may be apparent later. Figure 7 shows the arsenic level in some of the contaminated sources and the

number of critically affected patients corresponding to that source. The Panchayat hand pump, with an arsenic level of 0.35 mg/l, has shown maximum number of patients as most of the people of the village have been using water from it for a long time.

We plan to undertake a prolonged study to find whether the concentration of arsenic in groundwater is decreasing or increasing. We also propose to investigate the reasons for presence of arsenic in this part of India. Unlike West Bengal and Bangladesh, the soil of this region is not alluvial in nature, which provides greater significance to this study.

We need to study the geo-chemical processes operating under the subsurface to evaluate the role of the redox phenomenon occurring at the sediment–water interface. The mobility of arsenic in a given area could be affected by many factors such as the redox conditions (Eh), pH, presence of the competing anions and complexing ions, salinity, clay content, grain size and composition of the soil and sediment, presence of other metal ions, and the non metals such as S and P in the system. Its transport and uptake may be further affected by groundwater flow rate, nature of the plume below the subsurface, contaminant phases (dissolved, adsorbed, etc.) and temporal variation of the above parameters[19–22]. Arsenic is reported to occur mainly in two forms in groundwater, i.e. as arsenopyrite (FeAsS), usually in clay–silt sequences or as adsorbed phases on to the Fe-oxyhydroxides[19,22]. Two mechanisms have been proposed for the mobilization of arsenic at the sediment–water interface. First is that the pyrite could undergo chemical transformation under the influence of atmospheric oxygen releasing sulphuric acid and arsenic. This atmospheric oxygen becomes available under the subsurface due to excessive pumping and lowering of the groundwater table locally[23–25]. The second mechanism suggests that the iron oxide surfaces get positively charged at certain pH conditions and arsenate and arsenite may be sorbed as negatively charged ions. The arsenic adsorbed on to iron oxide coatings could be mobilized[26–28] under anaerobic conditions with reduction of the ferric iron to soluble ferrous iron and subsequent release of the arsenic. A recently published paper[29] reports high correlation between the diagenetically available iron and the arsenic concentration. Thus, the reduction of ferric iron should result in higher iron content in the groundwater as has been the case with most of the results on groundwater quality from the West Bengal and Bangladesh.

On analysing the data from the present location, it seems that both the above theories explain that arsenic in groundwater are not sufficient. This fact can be seen from the correlation study of the data obtained at this location (Table 6). It shows neither a strong positive correlation with the iron concentration nor a strong negative correlation with pH which are expected if the above theories of the genesis of arsenic in groundwater are applicable. This necessitates the study of the source profile and the geo-chemical reactions responsible for the occurrence of arsenic.

Figure 5. Planter keratosis (village Koudikasa).

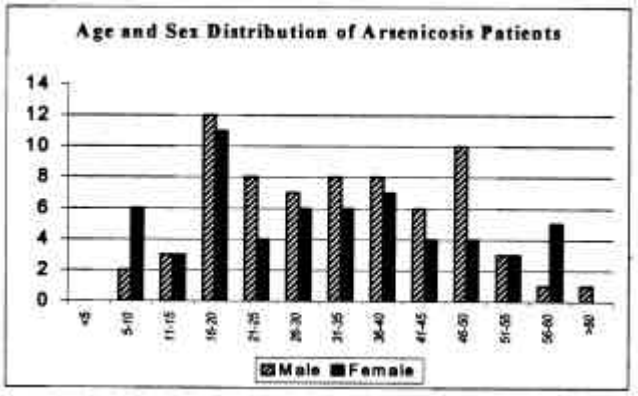

Figure 6. Age and sex of the very critically affected people in Koudikasa (n = 128).

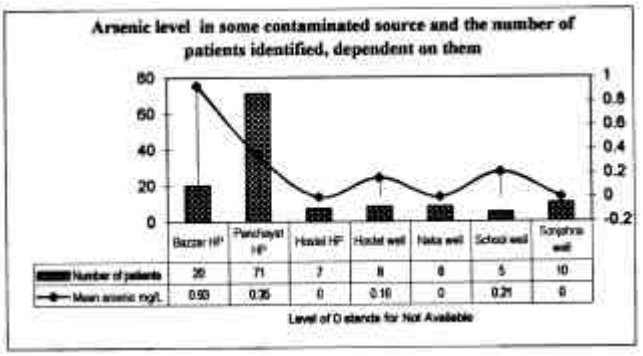

Figure 7. Arsenic level and number of arsenicosis patients.

Table 6. Correlation matrix obtained for the various water quality parameters studied

	pH	Total dissolved solids (DC)	Conductivity (m mhos)	ATC (m mhos)	Total hardness	Calcium	Magnesium	Sodium	Potassium	Alkalinity	Chlorides	Sulphates	Iron	Arsenic
pH	1.00													
TDS	0.70	1.00												
Conductivity	0.70	1.00	1.00											
ATC	0.70	1.00	1.00	1.00										
Hardness	0.77	0.67	0.65	0.65	1.00									
Calcium	0.83	0.89	0.89	0.89	0.88	1.00								
Magnesium	0.60	0.51	0.48	0.48	0.91	0.64	1.00							
Sodium	0.17	0.64	0.66	0.66	– 0.10	0.27	– 0.15	1.00						
Potassium	0.16	0.62	0.64	0.64	0.18	0.32	0.22	0.63	1.00					
Alkalinity	0.74	0.69	0.68	0.68	0.63	0.58	0.71	0.40	0.57	1.00				
Chlorides	0.53	0.93	0.93	0.93	0.54	0.85	0.29	0.61	0.50	0.38	1.00			
Sulphates	0.02	0.49	0.49	0.50	0.43	0.53	0.29	0.25	0.13	– 0.05	0.64	1.00		
Iron	0.12	– 0.31	– 0.30	– 0.31	– 0.28	– 0.18	– 0.45	– 0.33	– 0.25	– 0.27	– 0.25	– 0.70	1.00	
Arsenic	0.13	– 0.05	– 0.09	– 0.10	0.35	0.24	0.23	– 0.63	– 0.43	– 0.29	0.10	0.07	0.33	1.00

The groundwater of the Rajnandgaon district is quite rich in iron (Table 1) but the groundwater at Koudikasa has not shown an elevated level of iron. The inadequacy of the above two theories to account for arsenic at Koudikasa warrants special attention. Thus, the hypothesis of Nickson *et al*.[29] that the knowledge of the sedimentary architecture, and of the distribution of iron, arsenic and reductant carbon in Ganges alluvial sediments will enable a predictive model to be developed to guide future aquifer development in a way that minimizes arsenic pollution, may have a limited application.

Groundwater is continuously moving albeit slowly. Hence, aquifers hitherto uncontaminated may get contaminated in future. The district of Rajnandgaon is surrounded by some heavily populated districts like Durg, Raipur and Bilaspur, and there is an urgent need to address the problem.

These studies are also important since the mechanism of how the arsenic affects our bodies is not clearly known. In the Michigan area of USA, even the exposed population drinking contaminated water did not show much health problems. It is not clear whether the genetic composition, nutritional levels and climate play any role in arsenicosis. We came across six reported deaths because of arsenicosis, yet we do not have any method to ascertain this.

1. World Health Organisation, in *Arsenic in Drinking Water and Resulting Arsenic Toxicity in India and Bangladesh: Recommendations for Action*, 1997, SEA/EH/505.
2. Guha Mazumdar, D. N., Chakroborty, A. K., Ghose, A., Das Gupta, J., Chakroborti, D., Dey, S. B. and Chattopadhaya, N., *Bull. WHO*, 1988, **64**, 499–506.
3. Das, D., Chatterjee, A., Mandal, B. K., Samanta, G., Mandal, B. K., Roy Chowdhury, T., Samanta, G., Chowdhury, P. P., Chanda, C., Basu, G., Lodh, D., Nandi, S., Chakraborty, T., Mandal, S., Bhattacharya, S. M. and Chakraborti, D., *Analyst*, 1994, **119**, 168N–170N.
4. Chatterjee, A., Das, D., Mandal, B. K., Roy Chowdhury, T., Samanta, G. and Charkraborti D., *Analyst*, 1995, **120**, 643–650.
5. Das, D., Samanta, G., Mandal, B. K., Chowdhury, T. R., Chanda, C. R., Chowdhury, P. P., Basu, G. K. and Chakraborti, D., *Environ. Geochem. Health*, 1996, **18**, 5–15.
6. Bhattacharya, P., Chatterjee, D. and Jacks, G., *Int. J. Water Res. Dev.*, 1997, **13**, 79–92.
7. Ahmed, M., Brandstetter, A., Wenzel, W. W. and Blum, W. E. H., Proceedings of the Fourth International Conference on the Biogeochemistry of Trace Elements (eds Iskander, I. K., Hardy, S. E., Chang, A. C. and Pierzynski, G. M.), Berkeley, California 1997, pp. 263–264.
8. Dhar, R. K., Biswas, B. K., Samanta, G., Mandal, B. K., Chakraborti, D., Roy, S., Jafar, A., Islam, A., Ara, G., Kabir, S., Khan, A. W., Ahmed, S. A. and Hadi, S. A., *Curr. Sci.*, 1997, **73**, 48–59.
9. Chakraborty, A. K., Bannerjee, D., Ghoshal, S. and Barman, P., *Indian J. Med. Res.*, 1987, **85**, 326–334.
10. Tseng, W. P., Chu, H. M., How, S. W., Fong, J. M., Lin, C. S. and Yeh, S., *J. Natl. Cancer Inst.*, 1968, **40**, 453–463.
11. Tseng, W. P., *Environ. Health Perspectives*, 1977, **19**, 109–119.
12. Cebrian, M. E., Albores, A., Aquilar, M. and Blakely, E., *Human Toxicol.*, 1983, **2**, 121–133.
13. Robertson, F. N., *Environ. Geochem. Health*, 1989, **11**, 171–185.
14. Welch, A. H., Lico M. S. and Hughes, J. L., *Ground Water*, 1988, **26**, 333–347.
15. Strattan, G. and Writehead, H. C., *JAWWA*, 1962, **54**, 861.
16. National Environmental Engineering Research Institute, *Tech. Dig.*, 1977, **54**.
17. Greenberg, A. E., Clesceri, L. S. and Eaton, A. D. (eds), *Standard Methods for the Examination of Water and Wastewater*, American Public Health Association, Washington, 1992.
18. Mandal, B. K., Chowdhury, T. R., Samanta, G., Basu, G. K., Chowdhury, P. P., Chanda, C. R., Lodh, D., Karan, N. K., Dhar, R. K., Tamili, D. K., Das, D., Saha, K. C. and Chakraborti, D., *Curr. Sci.*, 1996, **70**, 976–986.
19. Bodek, I., Warren, J. L., Reehl, W. F. and Rosenblatt, D. H., *Environmental Inorganic Chemistry*, Pergamon Press, New York, 1988.
20. Robertson, F. N., *Environ. Geochem. Health*, 1989, **11**, 171–185.
21. Goldberg, S., *Am. J. Soil Sci. Soc.*, 1986, **50**, 1154–1160.
22. Korte, N. E. and Fernando, Q., *Crit. Rev. Environ. Control*, 1991, **21**, 1–39.
23. Bhattacharya, P., Chatterjee, D. and Jacks, G., in *Reaching the Unreached* (ed. John Pickford), 22nd WEDC Conference, New Delhi, September 1996, pp. 258–261.

24. Mallick, S. and Rajagopal, N. R., *Curr. Sci.*, 1996, **70**, 956–958.
25. Das, D., Basu, G., Chowdhury, T. R. and Chakraborty, D., in Proceedings of International Conference on Arsenic in Groundwater, Calcutta, 1995, pp. 44–45.
26. Saha, A. K. and Chakrabarti, C., in Proceedings of International Conference on Arsenic in Groundwater, Calcutta, 1995, p. 42.
27. De Vitre, R., Belzile, N. and Tessier, A., *Limnol. Oceanogr.*, 1991, **36**, 1480–1485.
28. Wilkie, J. A. and Hering, J. G., *Colloids Surf.*, 1996, **A107**, 97–107.
29. Nickson, R., McArthur, J., Burgess, W., Ahmed, K. M., Ravenscroft, P. and Rahman, M., *Nature*, 1998, **395**, 338.

Received 26 December 1998; revised accepted 26 May 1999

Male-sex-associated RAPD markers in *Piper longum* L.

N. S. Banerjee, P. Manoj and M. R. Das

Rajiv Gandhi Centre for Biotechnology, Jagathy, Thiruvananthapuram 695 014, India

***Piper longum* L., a medicinally important plant, showing a dioecious flowering pattern – plants bearing either male or female sex organs – was investigated for the molecular basis of genotypic differentiation between the male and female plants, using randomly amplified polymorphic DNA (RAPD) technique. Polymorphism in the genomic DNA of plants of twenty-five female and six males was analysed by RAPD, using 40 decamer random oligonucleotide primers. Two RAPD bands consistently appeared only in the plants showing male genotype, suggesting thereby the male-associated nature of these DNA markers in dioecious *P. longum*. So far, in this wild species of *Piper*, genetic or chromosomal basis of dioecy has not been reported. Perhaps, this is the first report – to the best of our information – on male-associated RAPD markers in *P. longum*.**

IN the medicinally important dioecious species, *Piper longum* L. (Sanskrit: *Pippali*), male and female plants mainly differ in the morphology of their spikes which bear minute achlamydous unisexual flowers. Mature female spikes, known as 'long pepper', are shorter and thicker than the male spikes (Figure 1). Long pepper has high demand for its medicinal properties and for its use in ayurvedic and traditional system of medicine in the treatment of respiratory tract diseases of humans[1]. Thus, like in many other dioecious species of plants, it would appear that the mechanism of sex determination has perhaps influenced the biosynthesis and accumulation of pharmacologically useful compounds in the female flower-bearing organ in this species as well. Thus, information on the genetic and molecular basis of the sex-determining mechanism in this species could provide insights on the genetic regulation of biosynthesis of such compounds, and eventually lead to undertaking of breeding programmes to manipulate the biosynthesis of such compounds.

Apparently, there is no common mechanism of sex determination in dioecious plants, constituting about 4% of all angiosperms. While sex determination by heteromorphic sex chromosomes (X and Y), as in higher animals, has been reported in plants like *Silene latifolia* and *S. dioeca*[2–7] – in literature, so far five families, belonging to angiospermic group, show this mechanism of sex determination – in wood sorrel (*Rumex latifolia*) and some other plants, sex of an individual plant is determined by dosage compensation mechanism based on the ratio of X chromosome to autosome[8]. However in *P. longum*, karyotype studies have not revealed the presence of such heteromorphic sex chromosomes, and researchers have differed on its diploid chromosome number[1] (24 to 96). Furthermore, epigenetic control of sex determination, operating in some plant species like *Mercurials annua*, *Cannabis sativa*, and *Arisaema triphyllum*,[9–11] perhaps does not control sex determination in *P. longum* where male and female plants strictly maintain their respective sexual phenotypes. This indicates clear genetic basis of difference between the male and female individuals of this species.

In the absence of information on chromosomal and genetic basis of sex determination, therefore investigation of molecular basis of genetic differentiation between the male and female genotypes was considered worth exploring. Sex-linked genetic markers could not only be useful in breeding programmes but would also allow the understanding of the genetics of dioecism in *P. longum*. Therefore, we examined such differences using randomly amplified polymorphic DNA (RAPD) technique[12,13]. Normally, since *P. longum* is propagated vegetatively, though fertile male and female flowers are produced by the plants, progeny of male and female plants from a cross between known parents was not available for this study. Hence, to study genetic differences in male and female plants, a germplasm collection, consisting of 25 female and 6 male entries, collected from geographically isolated regions, was analysed.

Plants were grown and maintained in the experimental garden at the R.G. Centre for Biotechnology, Trivandrum. Total genomic DNA was isolated from young healthy leaves, following the standard protocol[14]. The purified genomic DNA was subjected to polymerase chain reaction (PCR) for RAPD analysis, using random decamer oligonucleotide primers (OPA-1 to OPA–20 and OPAC-1 to OPAC-20), courtesy M/S Operon Inc., USA. The genomic DNA from different plants (20 ng each) was subjected to PCR in the presence of 20 mM Tris-HCl (pH 9.0), 50 mM KCl, 1.5 mM $MgCl_2$, 200 µM each of dNTPs, 15 picomole primer, and 0.5 unit of Taq DNA polymerase (M/S Bangalore Genei, India). Total volume of the reaction

*For correspondence. (e-mail: rgcbt@md2.vsnl.net.in)

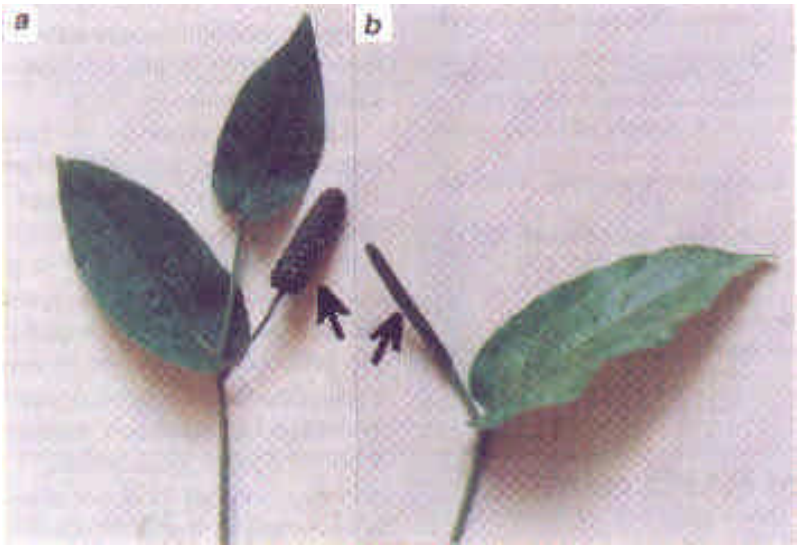

Figure 1. Spike-bearing twigs of: ***a***, female plants; and ***b***, male plants. Arrow heads indicate their spikes.

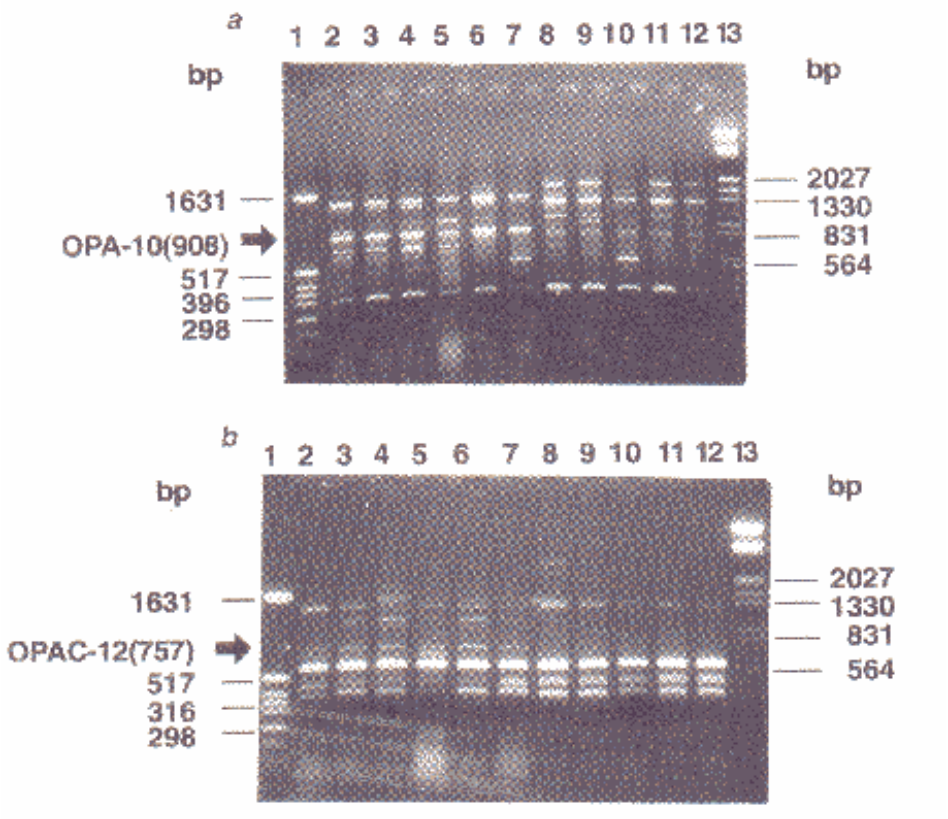

Figure 2. Fractionation of RAPD products developed by: (***a***) primer OPA-10 and (***b***) primer OPAC-12 from total genomic DNA of male and female plants of *P. longum* on 1.2% agarose gel. Lane 1; *Hind*I-digested pBR322 DNA (DNA molecular weight marker): Lanes 2 through 7; RAPD products from DNA of different male plants: Lanes 8 through 12; RAPD products from DNA pools (FP1 to FP6, text) of different female plant entries: Lane 13; Lambda DNA digested with *Eco*RI and *Hind*III (DNA molecular weight marker). Arrow heads indicate male-related RAPD bands, OPA-10 (908) and OPAC-12 (757), in ***a*** and ***b*** respectively.

mixture was made to 20 µl, and overlayed with 30 µl mineral oil, procured from Sigma. PCR was carried out in a Perkin-Elmer (PE480) thermal cycler. For the detection of genetic differences among the individual plants, the PCR programme was carried out stepwise as: initial denaturation at 94°C for 4 min; 40 cycles of denaturation at 94°C for 45 sec, followed by annealing at 37°C for 45 sec and polymerization at 72°C for 90 sec; and final extension at 72°C for 7 min. For identifying sex-related genetic differences, the PCR programme was slightly modified. After the initial denaturation step; 40 cycles of denaturation at 94°C for 1 min, followed by annealing at 40°C for 1 min; and extension at 72°C for 2 min, followed by final extension at 72°C for 7 min. PCR products were fractionated on 1.2% agarose gel in 1X Tris-borate-EDTA buffer. The gels were stained in 0.01% ethidium bromide[15].

The experiment was carried out in two stages. In the first stage, genetic differences among the six male and four female entries of *P. longum* L. were investigated using 40 RAPD primers. Successful amplification of RAPD bands from all the lines was obtained with 36 primers. This allowed us the comparison of 398 RAPD bands and identification of 10 primers, which produced probable male-related RAPD bands. While these bands (14) were amplified from the genomic DNA of all the male entries, they were absent in the similar PCR products of the tested four female entries.

In the next stage, to confirm for the absence of these fourteen RAPD bands, in all the available female entries, we examined genomic DNA from all the 25 entries by pooling these into five different groups (each pool containing equal amounts of DNA from five different plants). RAPD profiles of the five pools of DNA, both from the female plants and the six male plants were developed with selected primers and compared.

A 908-bp band, OPA-10 (908), amplified by OPA10 (5′-GTGATCGCAG-3′) primer and a 757-bp band, OPAC-12 (757), amplified by OPAC-12 (5′-GGCGA- GTGTG-3′) primer from genomic DNA of the six male entries were absent in the PCR products of the five pools of DNA from the female entries (Figure 2). These pools of female DNA represented all the 25 female plant entries available. Thus, within the limits of male and female genotypes available in this study, the two RAPD bands, OPA-10 (908) and OPAC-12 (757), appeared to be male-sex-related DNA markers in *P. longum.* Thus, analyses of sex-linked inheritance pattern, which is necessary for the confirmation of male specificity of these DNA markers, have been initiated. So far, sex-linked RAPD markers have been reported from two other plant species as well:

a 945-bp RAPD band, OPA-08 (945), was shown to be female specific in *Pistachio vera*[16]. Alstrom-Rapaport *et al.*[17] reported an RAPD band UBC354(560) which was probably linked to a sex determination locus in *Salix viminalis*. For the male-sex-associated genetic factors, Y-chromosome-specific restriction fragments[18] and genes[19–24] have been reported only from white campione (*Silene latifolia*). In the recent past, PCR amplification of a 900-bp male (Y-chromosome)-specific band representing a degenerate Y-linked homologue of a X-linked gene has also been reported in this species[24]. However, to the best of our knowledge, no report of male-sex-linked RAPD markers in dioecious flowering plants is available in the literature.

1. Viswanathan, T. V., in *Medicinal and Aromatic Plants* (eds Chadha, K. L. and Gupta, R.), Malhotra Publishing House, New Delhi, 1995, pp. 373–383.
2. Yampolski, C. and Yampolski, H., *Bibl. Genetics*, 1992, **3**, 1–62.
3. Parker, J. S., *Chromosomes Today*, 1990, **10**, 187–198.
4. Westergaard, M., *Hereditas*, 1946, **32**, 419–443.
5. Ye, D., Oliveira M., Veuskens, J., Wu, Y., Installe, P., Hinnisdaels, S., Truong, A. T., Brown, S., Mouras, A. and Negrutiu, I., *Plant Sci.*, 1991, **80**, 93–106.
6. Grant, S., Houben, A., Vyskot, B., Siroky, J., Pan, W.-H., Macas, J. and Saedler, H., *Dev. Genet.*, 1994, **15**, 214–230.
7. Farbos, I., Vcuskens, J., Vyskot, B., Oliviera, M., Hinnisdacls, S., Aghmir, A., Mouras, A. and Negrutiu, I., *Genetics*, 1999, **151**, 1187–1196.
8. Ainsworth, C., Crossley, S., Buchanan-Wollaston, V., Thangavelu, M. and Parker, J., *Plant Cell*, 1995, **7**, 1583–1598.
9. Louis, J. P., *J. Hered.*, 1989, **80**, 104–111.
10. Galoch, E., *Acta Soc. Bot. Pol.*, 1978, **47**, 135–161.
11. Policanski, D., *Proc. Natl. Acad. Sci. USA*, 1981, **78**, 1306–1308.
12. Welsh, J. and McClelland, M., *Nucleic Acids Res.*, 1989, **18**, 7218–7228.
13. Williams, J. G. K., Kubelik, A. R., Livak, K. J., Rafalskie, J. A. and Tingey, S. A., *Nucleic Acids Res.*, 1989, **18**, 6231–6235.
14. Rogers, S. O. and Bendich, A. J., *Plant Molecular Biology Manual* (eds Gelvin, S. B. and Schilperoort, R. A.), Kluwer, Dordrecht, 2nd edn, 1994, pp. 1–8.
15. Sambrook, J., Fritsch, E. F. and Maniatis, T., *Molecular Cloning: A Laboratory Manual*, Cold Spring Harbour Laboratory Press, Cold spring Harbour, New York, 1989.
16. Hormaza, J. L., Dollo, -L. and Polito, -V. S., *Theor. Appl. Genet.*, 1994, **89**, 9–13.
17. Alstrom-Rapaport, C., Lascoux, M., Wang, Y. C., Roberts, G. and Tuskan, G. A., *J. Hered.*, 1998, **89**, 44–49.
18. Donnison, I. S., Siroky, J., Vyskot, B., Saedler, H. and Grant, S. R., *Genetics*, 1996, **144**, 1893–1901.
19. Hardenack, S., Ye, D., Saedler, H. and Grant, S., *Plant Cell*, 1994, **6**, 1725–1737.
20. Matsunga, S., Kawano, S., Takano, H., Uchida H., Sakai, A. and Kuroiwa, T., *Plant J.*, 1996, **10**, 679–689.
21. Barbacar, N., Hinnisdaels, S., Farbos, I., Moneger, F., Lardon, A., Delichere, C., Mouras, A. and Negrutiu, I., *Plant J.*,1997, **12**, 805–817.
22. Scutt, C. P., Li, Y., Robertson, S. E., Malcolm, E., Willis, M. E. and Gilmartin, P. M., *Plant Physiol.*, 1997, **114**, 969–979.
23. Robertson, S. E., Li, Y., Scutt, C. P., Willis, M. E. and Gilmartin, P. M., *Plant J.*, 1997, **12**, 155–168.
24. Guttmann, D. S. and Charlesworth, D., *Nature*, 1998, **393**, 263–266.

ACKNOWLEDGEMENTS. Financial help from STED-SRF, project no. 90/98/STED, Government of Kerala, is acknowledged. We thank Dr K. T. Prasanna Kumari of Kerala Agriculture University, Thrissur, for allowing us to share the germplasm collection of *P. longum* entries for this study. We acknowledge valuable help and suggestions by Dr George Thomas and Dr Shaji Philip.

Received 11 June 1999; accepted 2 July 1999

Antifungal studies of some essential oils at various pH levels for betterment of antifungal drug response

Sushil K. Shahi*, Amritesh C. Shukla and Anupam Dikshit

Biological Product Laboratory, Botany Department, University of Allahabad, Allahabad 211 002, India

Antifungal evaluation of the stored essential oil of some *Eucalyptus* species, viz. *E. amygdalina, E. citriodora, E. dalrympleana* and *E. laveopinea* was tested against dermatophyte, viz. *Epidermophyton floccosum, Microsporum gypseum, M. nanum, Trichophyton mentagrophytes, T. rubrum* and *T. violaceum*. The efficacy of the oils increased for inhibiting the mycelial growth of test orgainsms by adjusting the pH of the media to 4, 7 and 9 from their normal pH of 5.6. The enhancement in the efficacy of various oils recorded as percentage changed in minimum fungistatic and minimum fungicidal concentrations. The minimum fungistatic and fungicidal concentrations decreased in the range from 12.5 to 80.0% and 11.1 to 75.0%, respectively against all the test organisms, except for the oil of *E. citriodora* which showed an increase of 25% in the minimum fungistatic concentration against *T. rubrum* and *T. mentagrophytes*. These oils at normal and alkaline pH inhibited heavy doses of inoculum potential. Moreover, oils did not show any adverse effect on mammalian skin up to 5% concentration at normal and alkaline pH.

SUPERFICIAL ringworm infections occur more frequently than subcutaneous and systemic mycoses and remain a therapeutic problem in tropical and subtropical countries, despite the availability of a number of antifungal ointments, paints, lotions and powders. Sources of these agents are largely nonrenewable petroproducts that are nonbiodegradable and cause adverse effects and residual toxicity[1]. Recently, some products of higher plant origin have been shown to be effective source of chemotherapeutic agents and provide renewable sources of useful antifungals of biodegradable nature which are devoid of side effects[1–3]. These findings prompted the exploration of other plant products that could be exploited as antifungals. In our preliminary screening, the essential oils extracted from fresh leaves of the *Eucalyptus* spp. and tested at 0.4 µl/ml were found to possess antifungal activity against dermatophytes[4], viz. *Microsporum gypseum* (Bodin) Guiart et Grigorakis, *Trichophyton mentagrophytes* (Robin) Blanchard and *T. rubrum* (Castellani) Sabouraud. The present communication describes detailed antifungal studies of the four effective stored essential oils of *Eucalyptus* spp., viz. *E. amygdalina* Labill, *E. citriodora* Hook, *E. dalrympleana* Maiden and *E. laveopinea* Baker with special attention to pH adjustment against test organisms, viz. *Epidermophyton floccosum* (Hartz) Langeron et Milochevitch, *Microsporum gypseum* (Bodin) Guiart et Grigorakis, *M. nanum* Fuentes, *Trichophyton mentagrophytes*, *T. rubrum* and *T. violaceum* Bodin which cause dermatophytoses in animals and human beings.

The oils were extracted from fresh leaves of four *Eucalyptus* spp. by hydrodistillation using Clevenger's apparatus[5] and tested at 1.0 µl/ml for their antifungal evaluation after storage for 10 years at 27 ± 5°C against the test organisms, viz. *E. floccosum*, *M. gypseum*, *M. nanum*, *T. mentagrophytes*, *T. rubrum* and *T. violaceum* by poisoned food technique[6] with slight modification[1].

The nature of toxicity, i.e. fungistatic/fungicidal along with the minimum effective concentrations (MECs) of the oils were ascertained by the method of Garber and Houston[7] with slight modification[1].

To study the effect of pH adjustment on the toxicity of the oil, the technique of Dikshit *et al.*[8] with slight modification[1], has been followed using citrate phosphate buffer[9] for pH 4 and 7, and boric acid–borax buffer[10] for pH 9. Two sets of culture media were prepared separately for control and treatments. In the test sets of pH 4, 7 and 9, requisite amount of the oil samples was mixed in acetone (2% of the required quantity of the medium) and then added into the sterilized Sabouraud dextrose agar (SDA) medium of respective pH levels. In controls of each buffered medium, the same volume of sterilized water (in place of the oil) and acetone was mixed in appropriate amounts.

Mycelial discs of 5 mm diameter, cut out from the periphery of 7-day-old culture of the test organisms were aseptically inoculated upside down on the surface of the SDA medium in plates. Inoculated petri plates were incubated at 27 ± 1°C and observations were recorded on the seventh day. Percentage of mycelial growth inhibition on different pH levels was calculated using eq. [I] of Shahi[1].

$$I = \frac{(c-t)\times 100}{c},$$

where I is % growth inhibition at adjusted pH, c is colony diameter at adjusted pH in controls, and t is colony diameter at adjusted pH in treatment.

The nature of toxicity, i.e. fungistatic/fungicidal of the oils at adjusted pH levels in treatments as well as in controls, was determined by reinoculating the inhibited discs on SDA medium (pH ± 5.6) in petri plates[1]. Fungal growth on the seventh day indicated fungistatic activity while its absence denoted fungicidal nature. Percentage of changed minimum static concentration (CMSC) as well as changed minimum cidal concentration (CMCC) of the oils at adjusted pH levels 4, 7 and 9 was calculated following the equations of Shahi[1].

$$Cs\ (\%) = \frac{(S-s)\times 100}{S},$$

where Cs is % change in minimum static concentrations, S is

*For correspondence.

minimum static concentration at normal pH, and *s* is minimum static concentration at adjusted pH.

$$Cc\ (\%) = \frac{(C - c) \times 100}{C},$$

where *Cc* is % change in minimum cidal concentrations, *C* is minimum cidal concentration at normal pH, and *c* minimum cidal concentration at adjusted pH.

The effect of inoculum density at normal and alkaline pH (increased progressively up to 30 discs in multiples of 5 and each of 5 mm diameter) of various test organisms on toxicity of the oils, was determined following the procedure outlined by Dikshit and Dixit[11] using the agar- free medium as adopted by Pandey *et al*.[12].

To see the irritant activity, if any, of the oils by their topical application on human skin at normal and alkaline pH 9, requisite quantity of the oil sample was mixed in PEG 400 LR and then the pH was adjusted using NaOH drop by drop with constant stirring[1]. The experiment was carried out following the patch test method of Roxburgh and Borrie[13].

All the four oils at 1.0 µl/ml inhibited 100% mycelial growth for all the organisms tested. The minimum static concentrations (MSCs) of oil from *E. amygdalina* ranged from 0.5 to 0.9 µl/ml, *E. citriodora* from 0.4 to 0.9 µl/ml and *E. laveopinea* from 0.3 to 0.4 µl/ml depending upon the test organisms while that of *E. dalrympleana* exhibited 0.3 µl/ml as the MSC for all the test organisms (Table 1) at the normal pH of the oils.

The minimum cidal concentrations of *E. citriodora* ranged from 0.8 to 1.0 µl/ml, *E. dalrympleana* and *E. laveopinea* from 0.5 to 0.8 µl/ml, depending upon the test organisms. The minimum cidal concentration of *E. amygdalina* could not be observed as it remained static at the concentrations tested (Table 2).

normal pH 5.6 which changed to 0.2 to 0.7 µl/ml at adjusted pH 4 and 7 against different test organisms (Table 3). In other words, the decrease in MSC ranged from 12.5 to 50.0%. However, the oil of *E. citriodora* showed an increase of MSC by 25% against *T. mentagrophytes* and *T. rubrum* at pH 7. Similarly, the MSCs of the oils of *E. laveopinea*, ranging from 0.3 to 0.5 µl/ml and of *E. dalrympleana*, at 0.3 µl/ml at normal pH 5.6 changed to 0.1 to 0.2 µl/ml. These differences in MSCs are statistically significant (Table 1). Their calculated decreased MSCs were found to be in the range 33.3–75.0%, 50.0–80.0% and 33.3–66.6%, respectively against various dermatophyte at adjusted pH levels 4 and 7. The MSCs at pH 9 could not be considered due to absence of mycelial growth in controls. Further, it was confirmed that higher pH (pH 9) checked the growth of the fungi but did not kill it, i.e. the effect was fungistatic (Table 4).

The minimum fungicidal concentrations of *E. citriodora*, *E. dalrympleana* and *E. laveopinea* ranged between 0.5 and 1.0 µl/ml at normal pH, changed to 0.2–0.9 µl/ml at pH 4, 7 and 9 (Table 2), thereby percentage of decreased minimum cidal concentration ranged between 11.1 and 75.0 at the pH of 4, 7 and 9 with different test organisms. Unlike the aforementioned oils, the effect of the oil of *E. amygdalina* remained static at the normal pH 5.6 as well as at pH 7. However, at altered pH 4 and 9 their minimum cidal concentrations were found to be variable between 0.6 and 0.8 µl/ml with different test organisms. On comparing the MSCs at normal pH 5.6, the essential oils of all the species of *Eucalyptus* withstood heavy doses of inocula, exhibiting 100% mycelial growth inhibition at their respective MSCs of various test organisms at normal and alkaline pH 9, and the oils did not show any irritation or adverse effect on mammalian skin up to 5% concentration at normal and alkaline pH 9.

Table 1. Minimum static concentration (µl/ml) with no mycelial growth on the essential oil of *Eucalyptus* spp. at normal and adjusted pH levels

	Essential oils of *Eucalyptus* spp. tested at various pH levels											
	E. amygdalina			*E. citriodora*			*E. dalrympleana*			*E. laveopinea*		
Fungi[a]	4	5.6[b]	7	4	5.6[b]	7	4	5.6[b]	7	4	5.6[b]	7
Ef	0.4	0.5	0.4	0.6	0.9	0.7	0.1	0.3	0.2	0.2	0.3	0.15
Mg	0.5	0.9	0.7	0.7	0.9	0.5	0.1	0.3	0.1	0.1	0.3	0.15
Mn	0.4	0.6	0.5	0.7	0.8	0.7	0.1	0.3	0.2	0.1	0.4	0.15
Tm	0.5	0.8	0.7	0.2	0.4	0.5	0.1	0.3	0.1	0.1	0.4	0.1
Tr	0.5	0.8	0.7	0.2	0.4	0.5	0.1	0.3	0.2	0.1	0.3	0.15
Tv	0.5	0.9	0.7	0.7	0.9	0.5	0.1	0.3	0.1	0.2	0.4	0.1
P value[c]	5.9	6.3		7.7	3.6		0.0	8.9		7.5	7.5	

[a]*Ef*, *Epidermophyton floccosum*; *Mg*, *Microsporum gypseum*; *Mn*, *Microsporum nanum*; *Tm*, *Trichophyton mentagrophyteis*; *Tr*, *Trichophyton rubrum*; *Tv*, *Trichophyton violaceum*.
[b]Normal pH of the medium.
[c]T test for pH differences.
Tabulated value at $p = 0.05$ is 2.23 for 6 d.f.

The MSCs of *E. amygdalina* and *E. citriodora* ranged from 0.5 to 0.9 µl/ml and 0.4 to 0.9 µl/ml, respectively at

Very few antifungal substances are available in the market when compared to antibacterial ones and they are

also relatively unsatisfactory in controlling the lesions produced by fungal organisms[13]. Stock[14] emphasized the need of powerful and specific antimycotic agents on an increasing scale to combat fungal infections. Discovery of essential oils exhibiting narrow or wide range of antifungal activity, as suggested in the present investigation, may prove useful in the development of effective antidermatophytic substances. Most workers in India have so far studied antifungal activity of candidate substances employing qualitative assay techniques[15,16] and have not described the nature of toxic action (fungistatic/ fungicidal) encountered with such materials.

In the earlier study of the *Eucalyptus* spp. fresh oil was used by Dikshit[4]. Unlike the essential oil of *Adenocalymma allicea* where its fungitoxicity expired after 21 days[17], the present study was conducted with oils stored for 10 years which were quite effective against the tested dermatophytes, in contrast to plant pathogenic and other fungi, viz. *Alternaria alternata*, *Aspergillus flavus* and *Penicillium italicum* (Shahi, unpublished). Therefore, the fungitoxic stability of the oil has been found to be organism-dependent. Hence, fresh oils can easily be used for developing an ointment without any fear of expiry.

In the present investigation, the minimum static/cidal concentrations of all the oils were determined except the oil of *E. amygdalina* which remained static at all the tested concentrations (Table 2). Thus, the oils may be strictly fungicidal or fungistatic or their nature may be dose-dependent. Further, the variations in minimum fungistatic concentration among the various *Eucalyptus* spp. against the test organisms are probably due to variations in the cineole contents (27–78%), the major constituent of essential oils as suggested by Singh *et al*.[18].

During pH adjustment studies, absence of growth in control sets (at pH 9) makes this part of the experiment apparently insignificant. But reinoculating the inhibited discs of control and test sets revealed the expression of differential activity, i.e. pH 9 is inhibitory in controls with fungistatic action while pH 9 along with required concentrations of the oils exhibited fungicidal nature. As such, it is significant to extend the test further instead of discarding it at a preliminary level. In an earlier study, the toxicity of the oils of *Cedrus deodara* and *Mentha arvensis* increased at adjusted pH levels against the plant pathogen *Helminthosporium oryzae*[8].

An ideal drug for topical application should not cause any irritation or burning effect on human skin. Therefore, the oils were tested for their irritant activity, if any, on mammalian skin at their normal and alkaline pH. Since the oils showed increased antifungal activity at pH 9 during *in*

Table 2. Percentage of changed minimum static concentration of the essential oil of *Eucalyptus* spp. at adjusted pH levels

	Essential oils of *Eucalyptus* spp. tested at various pH levels											
	E. amygdalina			*E. citriodora*			*E. dalrympleana*			*E. laveopinea*		
Fungi[a]	4	7	9	4	7	9	4	7	9	4	7	9
Ef	20.0	20.0	–	33.3	22.2	–	66.6	33.3	–	33.3	50.0	–
Mg	44.4	22.2	–	22.2	44.4	–	66.6	66.6	–	66.6	50.0	–
Mn	33.3	16.0	–	12.5	12.5	–	66.6	33.3	–	75.0	62.5	–
Tm	37.5	12.5	–	50.0	– 25	–	66.6	66.6	–	75.0	75.0	–
Tr	37.5	12.5	–	50.0	– 25	–	66.6	33.3	–	66.6	50.5	–
Tv	44.4	22.2	–	22.2	44.4	–	66.6	66.6	–	50.0	75.0	–

[a]*Ef, Epidermophyton floccosum*; *Mg, Microsporum gypseum*; *Mn, Microsporum nanum*; *Tm, Trichophyton mentagrophyteis*; *Tr, Trichophyton rubrum*; *Tv, Trichophyton violaceum.*
– , Not considered.

Table 3. Minimum cidal concentration (µl/ml) of the essential oil of *Eucalyptus* spp. at normal and adjusted pH levels

	Essential oils of *Eucalyptus* spp. tested at various pH levels															
	E. amygadalina				*E. citriodora*				*E. dalrympleana*				*E. laveopinea*			
Fungi[a]	4	5.6[b]	7	9	4	5.6[b]	7	9	4	5.6[b]	7	9	4	5.6[b]	7	9
Ef	–	–	–	0.8	0.9	–	–	0.7	0.8	–	–	0.4	–	–	–	0.3
Mg	0.7	–	–	0.8	0.8	–	–	0.6	0.8	–	–	0.4	0.5	–	–	0.3
Mn	–	–	–	0.8	0.8	0.9	–	0.6	0.4	0.5	–	0.5	–	–	–	0.3
Tm	0.7	–	–	0.7	0.3	0.8	–	0.2	0.6	0.8	–	0.4	0.2	0.8	0.6	0.3
Tr	–	–	–	0.6	0.6	1.0	0.7	0.4	0.6	0.8	0.7	0.4	0.4	0.5	0.3	0.3
Tv	0.7	–	–	0.7	0.8	–	–	0.6	0.4	0.8	–	0.4	0.2	0.8	–	0.3

[a]*Ef, Epidermophyton floccosum*; *Mg, Microsporum gypseum*; *Mn, Microsporum nanum*; *Tm, Trichophyton mentagrophyteis*; *Tr, Trichophyton rubrum*; *Tv, Trichophyton violaceum.*
[b]Normal pH of the medium.
– , Remained static.

Table 4. Percentage of charged minimum fungicidal concentration of the essential oil of *Eucalyptus* spp. at adjusted pH levels

	Essential oils of *Eucalyptus* spp. tested at various pH levels								
	E. citriodora			*E. dalrympleana*			*E. laveopinea*		
Fungi[a]	4	7	9	4	7	9	4	7	9
Ef	–	–	–	–	–	–	–	–	–
Mg	–	–	–	–	–	–	–	–	–
Mn	11.1	–	33.3	20.2	–	0.0	–		
Tm	62.5	–	75.0	25.0	–	50.0	75.0	25.0	62.5
Tr	40.0	30.0	60.0	25.0	12.5	50.0	20.0	40.0	40.0
Tv	–	–	–	50.0	–	50.0	75.0	–	62.5

[a]*Ef*, *Epidermophyton floccosum*; *Mg*, *Microsporum gypseum*; *Mn*, *Microsporum nanum*; *Tm*, *Trichophyton mentagrophyteis*; *Tr*, *Trichophyton rubrum*; *Tv*, *Trichophyton violaceum*.
– , Remained static.

vitro investigation, they were tested for their irritant activity at pH 9. The oils did not produce any irritation or adverse effect up to 5% concentrations. It can be concluded that ointments prepared from the oils may be most effective at pH 9 without causing any irritation on the human skin. Therefore, the present study clearly demonstrates that the oils of *Eucalyptus* spp. hold good promise as antidermatophytic agents which could be used in therapeutic remedy against dermatophytoses on account of their various fungitoxic properties, viz. antifungal, long shelf life, can withstand heavy inoculum density, efficacy at various pH levels, wide range of activity and absence of any adverse effect. These results can be interpreted with caution. Although the *in vitro* susceptibility testing shows promising activity against commonly encountered dermatophytes, its clinical usefulness should be established by further studies. Hence, the oils can be easily used as ointments for better results to the control of fungal infection in human beings.

1. Shahi, S. K., D Phil. thesis, Allahabad University, Allahabad, 1997.
2. Beye, F., *Plant Res. Dev.*, 1978, **7**, 13–31.
3. Fawcett, C. H. and Spencer, D. M., *Annu. Rev. Phytopathol.*, 1970, **8**, 403–418.
4. Dikshit, A., *J. Indian Bot. Soc.*, (supl.), (abst.), 1988, **66**, 4.
5. Clevenger, J. F., *J. Am. Pharm. Assoc.*, 1928, **17**, 346.
6. Grover, R. K. and Moore, J. D., *Phytopathology*, 1962, **52**, 876–880.
7. Garber, R. H. and Houston, B. R., *Phytopathology*, 1959, **49**, 449–450.
8. Dikshit, A., Singh, A. K. and Dixit, S. N., *J. Antibact. Antifung. Agents*, 1981, **9**, 9–10.
9. Mellvaine, T. C., *J. Biol. Chem.*, 1921, **49**, 183.
10. Holmes, W., *Anat. Record*, 1943, **86**, 163.
11. Dikshit, A. and Dixit, S. N., *Indian Perfum.*, 1982, **26**, 216–227.
12. Pandey, M. C., Sharma, J. R. and Dikshit, A., *Flavour Fragrance J.*, 1996, **11**, 257–260.
13. Roxburgh, A. C. and Borrie, P., The English Language Book Soc. and H. K. Lewis and Co. Ltd, XII edition, 1973.
14. Stock, R., *Pharma Int.*, 1981, **2**, 232–236.
15. Kaul, V. K., Nigam, S. S. and Dhar, K. L., *Indian J. Pharm.*, 1976, **38**, 21–23.
16. Lahariya, A. K. and Rao, J. T., *Indian Drugs*, 1979, **16**, 150–152.
17. Chaturvedi, R., Dikshit, A. and Dixit, S. N., *Trop. Agric. (Trinidad)*, 1987, **64**, 318–322.
18. Singh, A. K., Bhattacharya, A. K., Singh, K., Dubey, R. K. and Kholia, R. C., *Indian For.*, 1983, **109**, 153–158.

ACKNOWLEDGEMENTS. We thank the Head, Department of Botany, University of Allahabad for providing facilities; Dr Uma Banerjee, Division of Microbiology, All India Institute of Medical Sciences, New Delhi, India and Dr Gaillain Medgely, Department of Medical Mycology, St John's Institute of Dermatology, St Thomas Hospital, London, UK for providing the culture of dermatophytes and CSIR, New Delhi, for financial assistance.

Received 28 December 1998; revised accepted 24 February 1999

Two-dimensional NMR spectroscopic study of fibroblast and fibrosarcoma cell lines

B. Jayashree, K. R. R. Rajalaksmi, S. Deshmukh and T. Rajkumar*

Cancer Institute (WIA), 18, Sardar Patel Road, Adyar, Chennai 600 036, India

Two-dimensional NMR spectroscopy has been used to study a fibroblast (MRC-5) and human fibrosarcoma cell lines (HFS-9 and HT-1080). The cell lines were graded based on their tumorigenic characteristics in nude mice, and the synthetic phase fraction of their cell cycle. Analysis of the spectra from cells suggests an increase in the levels of lipids, metabolites and resonance patterns attributed to fucosylated antigens as a function of increasing tumorigenicity. The paper discusses the use of one- and two-dimensional ^{1}H NMR techniques in the gradation of fibrosarcoma cells and in differentiating them from the normal homologue, namely fibroblast cells.

SOFT tissue tumours/sarcomas are a heterogenous group of tumours that arise as soft tissue masses and usually exhibit the differentiated features of adult soft tissue, although in some cases there is no clearly defined normal tissue homologue. Soft tissue includes smooth and striated muscle, fat, fibrous tissue and the vessels that serve these tissues. These tumours can occur anywhere in the body and at any age although the distribution varies according to the histological type. Benign tumours are at least 100 times more common than their malignant counterparts and represent the most common group of human neoplasms[1]. Among the cases diagnosed annually at the Cancer Institute, leiomyosarcomas, fibrosarcomas and malignant fibrous histiocytomas are the most common, while in

*For correspondence. (e-mail: caninst@md2.vsnl.net.in)

children rhabdomyosarcomas are the most commonly detected soft tissue tumours. The overall survival of the treated non-metastatic patients is approximately 50%. The benefits that would be achieved if there were early means of detection are many. Mutilating surgery and mortality could be avoided. A non-invasive method for detection would be of even greater advantage.

This study aims to use NMR spectroscopy to investigate soft tissue tumours. As with any other study, the usefulness of the technique has been first demonstrated in cells and then in tissues. Soft tissue tumours such as fibrosarcomas arise from fibroblastic cells and their benign counterpart is the fibroma. This paper discusses the use of one- and two-dimensional purged correlated spectroscopy on human fibroblasts and fibrosarcoma cells.

The human fibrosarcoma cell lines HFS-9 and HT-1080 were obtained from National Facility for Animal Tissue and Cell Culture (NFATCC), Pune. The three cell lines were cultured under identical conditions in DMEM supplemented with 10% fetal bovine serum (Sigma, USA) and antibiotics: penicillin 10,000 units/ml, and streptomycin 10 mg/ml grown in a 10% CO_2 environment. Flow cytometry was done to characterize the grade of the two malignant cell lines based on their DNA content in the 'S' phase of the cell cycle (S phase fraction or SPF)[2], using the DNA cycle test plus kit from Becton Dickinson. The analysis was done on a Becton Dickinson FACScan flow cytometer. About $4–5 \times 10^6$ cells were injected subcutaneously in nude mice and the mice were kept under observation for growth of tumours for two months (6 mice per cell line) to test for tumorigenicity of the cell line. The cell cycle fractions and tumorigenic characteristics of the tumour cell lines used in this study are listed in Table 1. HT-1080, with a higher SPF and increased tumorigenicity (producing tumours within 8 days) has been classified as high grade relative to HFS-9. The cell lines were also analysed for their whole cell protein, lipid, triglyceride, phospholipid, cholesterol and cholesteryl ester content by standard biochemical procedures.

All the nuclear magnetic resonance spectroscopy experiments on cells were carried out on a JEOL-GSX-FT 400 MHz NMR spectrometer. A standard 5 mm probe head was used with the sample spinning at 15 Hz. For each experiment 10^8 cells were counted on a Neubauer slide before centrifuging and suspending in 0.4 ml PBS/D_2O. The residual water signal was suppressed using Delays Alternating with Nutations for Tailored Excitation (DANTE) sequence. The spectra were acquired over a spectral width of 8000 Hz using 32 K data points with a pulse delay of 3.2 s. A 11.5 µs excitation pulse was applied and 256 transients were acquired. An exponential window function with a line broadening of 3 Hz was applied to the data prior to Fourier transformation. Tri silyl propione sulfonate (TSPS) was used as the reference.

The purged correlation spectroscopy technique was used on cells, one thousand data points were collected in the t_2 dimension and 256 data points in t_1 dimension over a spectral width of 4000 Hz. Total experimental time for a PCOSY experiment consisting of 256 t_1 increments with 32 transients each was found to be less than 4 h. PCOSY matrices were zero filled to 512 points in t_1. The sinebell window function was applied in the t_1 and t_2 domains and Fourier transformed. The one-dimensional spectra were collected before and after the 2D spectra to check for sample stability. The spectra shown are representative of the three cell lines. One-dimensional and two-dimensional experiments were carried out on each cell three times and results were drawn only after the three spectra were found to be identical.

Table 1. Cell cycle phase and tumorigenic characteristics

Cell line	%G_1	%S	%G_2 + M	G_1CV	Tumorigenicity
HFS-9	69.22	16.69	14.09	4.7	Moderate (20 days,
HT-1080	65.3	25.3	9.4	12.3	5/6)
					Strong (8 days, 6/6)

G_1, G_1 phase of cell cycle; S, Synthetic phase of cell cycle; M, Mitotic phase of cell cycle; CV, coefficient of variation

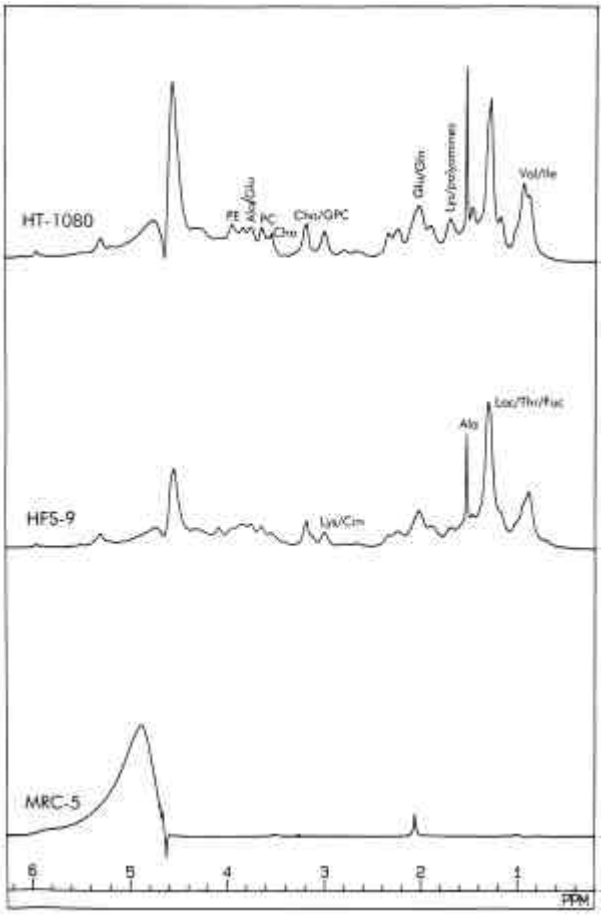

Figure 1. One-dimensional proton NMR spectra of 10^8 cells in 400 µl PBS in D_2O at 37°C. 256 transients were accumulated in the FID. An exponential window function with a line broadening of 3 Hz was applied prior to Fourier transformation. The spectra are plotted on a constant vertical scale (absolute intensity mode).

The proton 1D NMR spectra of the three cell lines are presented in Figure 1. The spectra of the fibroblast and fibrosarcoma cell lines are dominated by signals from fatty acid chains of lipid with resonances from methyl groups (–CH_3–) appearing at 0.9 ppm, methylene (–CH_2–) at 1.3, 1.6, 2.0 and 2.3 ppm. The olefinic group (–CH=) resonances are at 5.3 ppm. The resonance at 3.2 ppm is from the $N(CH_3)_3$ group of choline, phosphocholine and glycerophosphocholine[3]. Contributions from the resonances of carbohydrates, amino acids and phospholipid precursors are in the region 3.5–4.5 ppm of the spectrum. Qualitative differences are seen in the 1D spectra of the three cell lines, with a noticeable increase in the intensity of resonances in the spectra from bottom to top, i.e. from the fibroblast cell line to the high grade HT-1080. The resonances near 0.9 ppm and 1.3 ppm increase in intensity. The resonances at 1.5, 2.05, 2.2 and 2.8 ppm are seen to increase in the ascending order of the series. The abbreviation Fuc stands for contributions from fucose and Crn from creatine.

The PCOSY spectra of the three cell lines are shown in Figure 2 *a*–*c*. Chemical shift assignments of the cross peaks from triglyceride were made based on the assignment of plasma membrane triglyceride and triolein in $CDCl_3$ by Holmes and Mountford[4]. Those of phospholipid metabolites choline, phosphocholine (PC), phosphoethanolamine (PE) and glycerophosphocholine (GPC), free amino acids and peptides were based on the assignments of Sze and Jardetzky[5] and fucose (Fuc) from our spectrum of fucose and the assignments of Lean *et al*.[6].

An increase in the number and size of off-diagonal cross peaks is observed in the PCOSY spectra of the cell lines with increasing tumorigenicity. Some of the cross peaks from triglyceride namely B, E and F are identifiable only in

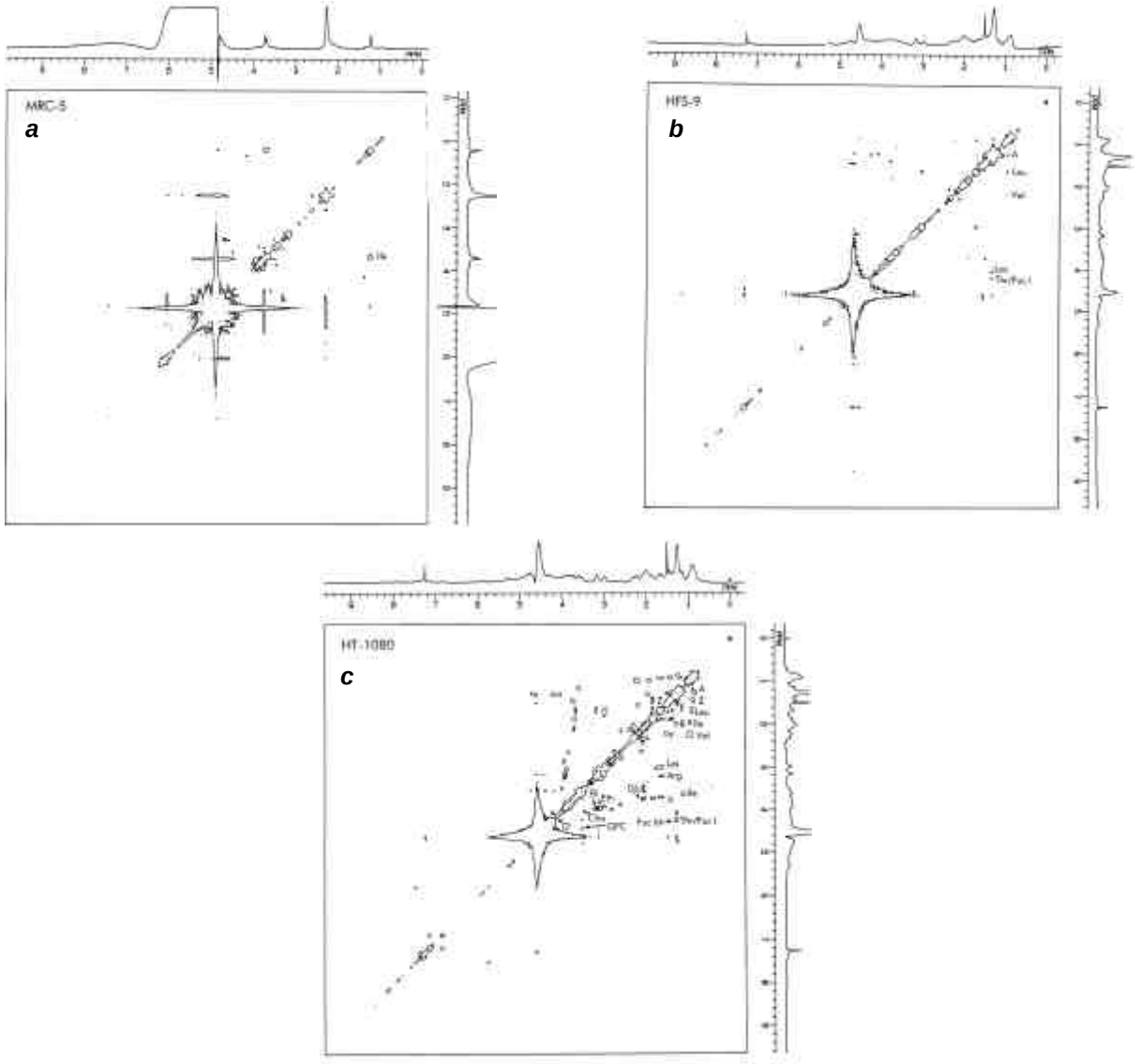

Figure 2. 400 MHz ^{1}H PCOSY spectra of 10^6 cells in 400 µl PBS in D_2O at 37°C. ***a***, MRC-5; ***b***, HFS-9; ***c***, HT-1080. A sine bell window function was applied in the t_1 and t_2 domains prior to Fourier transformation. The contour plots use the same absolute intensity scaling and the same contour levels.

Table 2. Whole cell chemical composition

ine	MRC-5	HFS-9	HT-1080
l protein (mg/10^8 cells)	9.86 ±0.2	11.1 ±1.1	11.56 ± 1
l lipid (mg/10^8 cells)	5.0 ± 1	6.1 ± 0.1	6.9 ± 1.2
pholipid (nmol/mg lipid)	210 ± 29	864 ± 27	1219 ± 41
cholesterol (nmol/mg lipid)	205 ± 24	611 ± 30	714 ± 15
esteryl ester (nmol/mg	ND	31 ± 3	54.5 ± 7
ylglycerol (nmol/mg lipid)	111 ± 7	230 ± 20	299 ± 9

HT-1080, so also those of phospholipids such as, phosphoethanolamine (PE), ethanolamine (Eth), choline (Cho) and glycerophosphocholine (GPC). The spectrum from MRC-5 shows only a single cross peak from amino acid isoleucine. These results are of significance because they reflect the growth rate of the cells. Malignant cells are associated with increased glycolytic rate, hence lactate is seen only in the PCOSY spectra of the tumour cell lines. Even the most slowly growing tumours possess a glycolytic capacity far in excess of the cells from which they have arisen. A high capacity of glycolysis is apparently necessary to maintain high concentrations of metabolic intermediates that can be used as precursors for macromolecular synthesis. Besides increased lactate, increased lipids such as triglyceride and phospholipids have also been reported[7]. The chemical composition of the three cell lines is presented in Table 2, which also shows an increase in the levels of these lipids with increasing grade. There is a need for enhanced phospholipid metabolism to support cell division and signal transduction events associated with phospholipid hydrolysis and changes within the plasma membrane responsible for invasion, metastasis and expression of growth factor receptors. A large increase in phosphocholine has been shown to be one of the earliest responses of tumour cells to growth factors[7]. Phosphoethanolamine may play an important role in the modification of membrane shape in malignant cells. Substantial alterations to the plasma membrane also occur, with drastic changes in the quantity and type of surface glycolipids and glycoproteins[8]. In colorectal cell lines, levels of fucosylated antigens have been found to correlate with grade, and the αL (Fuc1 → 2) βDGal linkages common to these antigens were identified as a likely source for the H5–H6 couplings of fucose seen in the 2D spectra of colorectal cells[6]. In the fibrosarcoma cells too, HFS-9 has a single cross peak at 1.33, 4.27, while HT-1080 has two cross peaks in this region corresponding to FucI and FucIII (1.33, 4.27 and 1.41, 4.3 ppm, nomenclature of Lean *et al*.[6]). A similar finding in mouse fibrosarcoma cell lines has been reported earlier by us[9]. Literature reports on the presence of saccharide antigens in sarcomas are restricted to studies on experimental animal tumours. There are no reports on the accumulation of fucosylated glycolipids. It would be of interest to see if tumour tissue also presents a similar two-dimensional spectrum, and then whether these cells and tissues are over-reactive for antibodies to these fucolipids/fucogangliosides (such as the blood group antigens Le^a, Le^b and Le^y).

Thus, one- and two-dimensional PCOSY techniques have been able to offer a gradation between fibroblast cells, intermediate grade fibrosarcoma and high grade fibrosarcoma cell lines. The gradation has been based on the identification of phospholipid, triglyceride cross peaks to a lesser extent, and cross peaks from membrane fucosylated antigens, which relate to grade and tumorigenicity of the cell lines. Similar studies on colorectal and breast cancer cells are available in the literature[3,6,10]. This is the first such study on fibrosarcoma cell lines. The clinical implication of this study is that ^{1}H NMR techniques may be used as an adjunct to conventional histology in the identification of the type of lesion (normal vs tumour, different grades of tumour) non invasively in soft tissue sarcomas like fibrosarcoma.

1. Cooper, S. C., *Adv. Cancer Res.*, 1993, **60**, 75.
2. Hidemann, W., Roesner, A., Wormann, B., Mellin, W., Klockenkemper, B., Boring, T., Buchner, T. and Grundman, E., *Cancer*, 1987, **59**, 324.
3. Mackinnon, W. B., Huschtscha, L., Dent, K., Hancock, R., Paraskeva, C. and Mountford, C. E., *Int. J. Cancer*, 1994, **59**, 248.
4. Holmes, K. T. and Mountford, C. E., *J. Magn. Reson.*, 1991, **93**, 407.
5. Sze, D. and Jardetzky, O., *Biochim. Biophys. Acta*, 1990, **1054**, 181.
6. Lean, C. L., Mackinnon, W. B., Delikatny, E. J., Whitehead, R. H. and Mountford, C. E., *Biochemistry*, 1992, **31**, 11095.
7. Cabello, J. R. and Cohen, J. S., *NMR Biomed.*, 1992, **5**, 226.
8. Hakomori, S-I., *Adv. Cancer Res.*, 1989, **52**, 257.
9. Jayashree, B., Visalakshi, V., Rajalakshmi, K. R., Sukumaran, M. S., Moni, M. S., Rajkumar, T. and Deshmukh, S., *Indian. J. Biochem. Biophys.*, 1998, **35**, 108.
10. le Moyec, L., Tatoud, R., Eugene, M., Gauville, C., Primot, I., Charlemagne, D. and Calvo, F., *Br. J. Cancer*, 1992, **66**, 623.

ACKNOWLEDGEMENTS. This project was supported by a DAE, Govt of India grant to the Institute. We thank RSIC (IIT), Chennai, for recording of high field NMR spectra.

Received 5 April 1999; revised accepted 16 June 1999